processes

MDPI

Article

Removal of Hexavalent Chromium Ions from Industrial Effluents Using Natural and Modified Diatomite, Taurite, Lewatit M500, and Activated Carbon

Bagdaulet Kenzhaliyev, Dametken Fischer *, Saniya Temirova, Almagul Ultarakova, Zhazira Baltabekova, Nauryzbek Bakhytuly and Kenzhegali Smailov

Institute of Metallurgy and Ore Beneficiation JSC, Satbayev University, Shevchenko Str., 29/133, Almaty 050010, Kazakhstan; bagdaulet_k@satbayev.university (B.K.); s.temirova@satbayev.university (S.T.); a.ultarakova@satbayev.university (A.U.); zh.baltabekova@satbayev.university (Z.B.); n.bakhytuly@satbayev.university (N.B.); k.smailov@satbayev.university (K.S.)
* Correspondence: d.fischer@satbayev.university; Tel.: +7-777-205-8875

Abstract: Hexavalent chromium Cr (VI) compounds present in ilmenite concentrate not only pose significant environmental hazards due to their toxicity but also complicate further processing, interfering with technological operations in industrial production. The high chromium content in ilmenite concentrates hinders their conversion into titanium-containing slag, necessitating the removal of chromium ions to permissible residual levels to produce titanium dioxide. In this study, various sorbents were investigated for the removal of chromate ions from the industrial effluents generated during ilmenite concentrate processing. The sorbents examined included natural and modified diatomite, activated carbon, taurite (shungite), and the ion-exchange resin Lewatit M500. The structures of both natural and modified diatomite were analyzed using scanning electron microscopy (SEM). It was determined that natural diatomite samples consist of diatom frustules of various shapes and their fragments, with structural element sizes ranging from submicron dimensions to 50 μm. A mathematical analysis of the sorption data for hexavalent chromium ion removal from solutions was performed. The results demonstrated high sorption efficiencies for Lewatit M500 (98.34%) and diatomite modified with iron compounds (98.95%). The findings suggest that diatomite is a promising sorbent for chromate ion removal from wastewater due to its availability and potential for chemical modification.

Keywords: industrial wastewater; chromium (VI) ions; sorption; diatomite; diatomite modification; activated carbon; taurite; ion-exchange resin; sorption isotherms

check for updates

Academic Editor: Andrea Petrella

Received: 23 January 2025
Revised: 7 March 2025
Accepted: 15 March 2025
Published: 26 March 2025

Citation: Kenzhaliyev, B.; Fischer, D.; Temirova, S.; Ultarakova, A.; Baltabekova, Z.; Bakhytuly, N.; Smailov, K. Removal of Hexavalent Chromium Ions from Industrial Effluents Using Natural and Modified Diatomite, Taurite, Lewatit M500, and Activated Carbon. *Processes* **2025**, *13*, 997. https://doi.org/10.3390/pr13040997

Copyright: © 2025 by the authors. Licensee MDPI, Basel, Switzerland. This article is an open access article distributed under the terms and conditions of the Creative Commons Attribution (CC BY) license (https://creativecommons.org/licenses/by/4.0/).

1. Introduction

The rapid expansion of industrial activities has significantly increased the presence of heavy metals in the environment. Among these, chromium (Cr) is one of the most prevalent pollutants, entering natural water bodies through various industrial wastewater discharges [1–4], including textile dyeing, leather tanning [5], and electroplating and metal-processing industries [6]. One of the most concerning forms of chromium pollution is hexavalent chromium (Cr(VI)), which is highly mobile, possesses strong oxidative properties, and can be absorbed through the skin. In aqueous environments, Cr(VI) primarily exists as chromate (CrO_4^{2-}) or dichromate ($Cr_2O_7^{2-}$) ions, depending on concentration and pH. Due to its structural similarity to sulfates, Cr(VI) can easily penetrate cell membranes, interact with intracellular components, and bind to DNA, leading to carcinogenic and other

toxic effects [7–10]. Given its high toxicity, effective measures must be implemented to reduce Cr(VI) concentrations to environmentally safe levels before its release into aquatic ecosystems. According to World Health Organization (WHO) guidelines, the maximum permissible concentration of chromium in drinking water is 0.05 mg/L, while the allowable discharge limit of Cr(VI) into surface waters is 0.2 mg/L [11,12]. However, natural attenuation mechanisms, such as adsorption onto minerals, are often ineffective, as Cr(VI) sorption decreases with increasing pH [13].

Various reduction and removal techniques have been explored to mitigate Cr(VI) contamination. Among these, the application of ferrous ions (Fe(II)), manganese ions (Mn(II)), sulfide-containing organic compounds, and sulfides has proven effective in converting Cr(VI) into its less toxic trivalent form. The efficiency of Fe(II)-mediated Cr(VI) reduction depends on the availability of different Fe(II) species, such as Fe(II), ferric hydroxyl ions ($FeOH^+$), and ferrous hydroxide ($Fe(OH)_2$) [14]. Additionally, studies have shown that Cr(III) can be oxidized rapidly by manganese dioxide (MnO_2) or gradually by atmospheric oxygen. Chromium adsorption onto hematite and goethite occurs predominantly through inner-sphere surface complexation in contrast to the ion-exchange mechanisms observed for α-aluminum oxide.

Beyond its environmental and health risks, chromium contamination also presents technological challenges in industrial production processes. For example, the presence of chromium in ilmenite concentrates complicates their further processing into titanium-bearing slag, making it necessary to remove the chromium to an acceptable residual concentration during titanium dioxide production. To meet industrial standards, slag used for technical-grade titanium dioxide must contain less than 0.3% chromium oxide and 9–12% iron compounds [15]. Given the increasing demand for effective and sustainable Cr(VI) removal methods, significant attention has been directed toward diatomite, a naturally occurring material with high porosity, large surface area, and chemical reactivity, making it a promising sorbent for chromium removal. Due to its availability, low cost, and environmental compatibility, diatomite has been widely explored as an alternative adsorbent for wastewater treatment. Kazakhstan possesses substantial diatomite reserves, particularly in the Aktobe region, yet these resources remain largely unexploited on an industrial scale. The Zhalpak diatomite field, for instance, features white diatomaceous cliffs up to 20 m high, forming a plateau covered by later sedimentary deposits, with estimated reserves of approximately 1.8 billion tons [16].

Diatomite, as a biogenic siliceous sedimentary rock, is composed mainly of amorphous silica (SiO_2). Its well-developed porous structure and high surface area contribute to its exceptional adsorption capacity [17]. The material's chemical reactivity is primarily attributed to the presence of active hydroxyl and acidic functional groups on its surface [18]. While diatomite is currently utilized in construction materials, fillers, and filtration media [19], its potential applications extend further, particularly in the removal of heavy metal ions from aqueous solutions [20,21]. Several studies have already demonstrated the feasibility of utilizing diatomite-based materials for a variety of environmental and industrial applications. Previous studies have investigated diatomite-based construction materials, iron oxide pigments, and reagents for the removal of hydrogen sulfide from wastewater [22–25]. A comparative study on the removal efficiency of Cr(VI) using natural diatomite and clay-containing diatomite revealed that at an initial Cr(VI) concentration of 0.5 mg/L at pH 2, clay-containing diatomite exhibited nearly 100% removal efficiency, whereas natural diatomite achieved only 28% efficiency [26]. However, it has been shown that unmodified diatomite lacks a strong adsorption capacity for heavy metal anions, including hydrogen chromate ions ($HCrO_4^-$), chromate ions (CrO_4^{2-}), and dichromate ions ($Cr_2O_7^{2-}$) in aqueous media [27]. To address this limitation, extensive research has

focused on chemical surface modifications of diatomite with iron compounds to enhance its sorption properties [28,29].

In addition to diatomite, various advanced sorbents have been investigated for Cr(VI) removal, including magnetite–diatomite nanocomposites synthesized via co-precipitation, which have demonstrated significant improvements in adsorption performance [30]. The effectiveness of these nanocomposites has been validated in industrial applications such as wastewater treatment in leather processing facilities. The incorporation of magnetite (Fe_3O_4) nanoparticles onto carbon microspheres enables the formation of outer-sphere complexes with Cr(VI) and facilitates its reduction to chromium (Cr(III)) [31]. Additionally, manganese oxide-modified diatomite (MnO_2-modified diatomite) has been shown to possess superior adsorption capabilities due to the well-dispersed manganese oxide particles within its porous structure [32,33].

MnO_2-modified diatomite has been explored for its enhanced adsorption capabilities, particularly in the removal of organic and inorganic contaminants from aqueous solutions. The surface of diatomite was functionalized with manganese dioxide (MnO_2) through chemical impregnation using acidic permanganate solutions followed by calcination. This modification resulted in an increased surface area and improved adsorption performance.

MnO_2-modified diatomite demonstrates dual functionality, facilitating both adsorption and oxidation mechanisms. Studies on aniline removal indicate that MnO_2-modified diatomite achieves a removal capacity of 42.9 mg/g, with FTIR and XPS analyses confirming that aniline is initially adsorbed onto the diatomite surface through hydroxyl (-OH) interactions before undergoing oxidative degradation mediated by MnO_2. This combined adsorption–oxidation mechanism enhances contaminant removal under mild conditions, positioning MnO_2-modified diatomite as a cost-effective adsorbent for wastewater treatment [34].

Additionally, MnO_2-modified diatomite has been studied for its efficiency in removing dyes from aqueous solutions. It incorporates δ-birnessite-type MnO_2, exhibiting high adsorption capacities for methylene blue (320 mg/g), reactive black (419 mg/g), and reactive yellow (204 mg/g). The adsorption mechanisms involve both the intercalation of dye molecules within the layered MnO_2 structure and surface adsorption onto MnO_2-modified diatomite. Structural analyses revealed minor shifts in XRD peaks due to dye intercalation, further supporting this dual mechanism [35].

Beyond naturally occurring materials, activated carbon (AC) adsorption remains one of the most widely used methods for the removal of heavy metals, including Cr(VI). AC is extensively employed due to its high surface area, porosity, and chemical modifiability. The efficiency of Cr(VI) removal by AC is influenced by multiple factors, including pH, surface chemistry, and adsorption kinetics. Studies have highlighted that Cr(VI) adsorption strongly depends on the solution pH, with optimal adsorption occurring in acidic environments, whereas alkaline conditions significantly reduce adsorption efficiency [36]. Cr(VI) adsorption on AC typically follows a pseudo-second-order kinetic model and is well described by the Langmuir isotherm, indicating monolayer adsorption. Additionally, Cr(VI) interacts with AC through electrostatic attraction and inner-sphere surface complexation, with strong binding observed at pH < 6 due to the dominance of $HCrO_4^-$ and $Cr_2O_7^{2-}$ species. At higher pH values, outer-sphere interactions dominate, leading to weaker adsorption [37]. A key aspect of AC performance is its reusability. Batch adsorption experiments have demonstrated that AC can maintain high Cr(VI) removal efficiency through multiple reuse cycles; however, progressive surface modification and functional group depletion lead to a gradual decline in adsorption capacity. Studies have reported a decrease in Cr(VI) removal efficiency from nearly 99.97% to approximately 43.37% after ten reuse cycles, emphasizing the need for periodic regeneration or surface modification to

sustain performance [38]. The functionalization of AC surfaces can significantly improve Cr(VI) adsorption efficiency. Modifications such as oxidation, impregnation with metal oxides, or the incorporation of nitrogen and sulfur functional groups enhance the surface affinity for Cr(VI), promoting selective adsorption. Hybrid adsorbents, combining AC with silica-based materials, have shown improved adsorption capacities due to the synergistic effect of increased surface functionalization [39]. However, the high cost associated with AC production limits its large-scale application.

Another alternative sorbent is taurite, a shungite-bearing rock from the Koksu deposit in Kazakhstan, which consists of highly dispersed silica oxide crystals embedded in an amorphous carbon matrix and has been explored for its sorption potential [40]. Shungite is a naturally occurring carbon-rich mineral known for its unique physicochemical properties, including electrical conductivity, catalytic activity, and sorption potential. The electrical conductivity and shielding effectiveness of shungite materials exhibit significant temperature-dependent behavior, with conductivity variations observed across a wide range of temperatures (77–300 K). Studies indicate that $\pi + \sigma$ plasmon energies correlate with changes in the frequency dependence of shielding effectiveness, highlighting the potential of shungite for electromagnetic shielding applications [41].

Shungite can be categorized into sodium- and potassium-rich varieties, which respond differently to chemical modifications such as acid, alkaline, and heat treatments. The application of these treatments alters the leaching behavior of undesirable elements and enhances shungite's adsorption capacity for dyes and heavy metals, including Ni, Cu, and Zn. Alkaline treatment has been shown to be the most effective for sodium-type shungite, while potassium-rich shungite benefits from acid and heat modifications, demonstrating the significance of tailored chemical processing for optimizing sorption performance [42].

Recent research has also explored the application of shungite for oil spill remediation. Mechanochemically activated shungite from the Koksu deposit (Kazakhstan) has demonstrated high oil sorption capacities, making it an effective material for mitigating petroleum contamination. The mechanochemical activation process, performed in planetary ball mills at varying rotation speeds and ball-to-sample ratios, significantly enhances the porosity and adsorption efficiency of shungite-based sorbents. Under dynamic conditions, shale-grade shungite exhibited an oil sorption capacity of 2.57–2.85 g/g, while under static conditions, sorption from 10% oil-contaminated soil samples reached 0.44–0.45 g/g over 60 days [43]. These findings highlight the potential for large-scale environmental cleanup operations using shungite-based materials.

The effectiveness of shungite as an adsorbent extends beyond heavy metals and dyes to uranium (VI) removal. Comparative analysis with other mineral and organic sorbents, including glauconite, diatomite, zeolite, peat, and coal-based adsorbents, has demonstrated that while peat and brown coal exhibit the highest sorption affinity for U(VI), shungite also displays notable adsorption performance [44]. Additionally, research into the leaching kinetics of Karelian shungite (types I–III) has provided insight into its chemical stability and catalytic behavior in water-treatment applications. Shungite exhibits pH-dependent dissolution properties with significant changes in elemental composition observed across the pH range of 1–12. Its catalytic activity in oxygen-rich environments suggests that shungite can play a role in advanced oxidation processes for water purification. The development of optimized shungite–carbonate filtration systems has further supported its potential as a cost-effective material for potable water treatment [45].

In addition to natural sorbents, the efficiency of strongly basic anion-exchange resins has been widely studied. The Lewatit MonoPlus M500 resin, a gel-type anion exchanger based on a styrene-divinylbenzene copolymer, has been successfully used for Cr(VI) removal due to its chemical and mechanical stability [46–49]. While anion-exchange resins

can be classified into strongly and weakly basic types [50], studies have shown that macroporous resins, such as Lewatit MP 64 and Lewatit MP 500, exhibit strong affinities for Cr(VI) removal from aqueous solutions [51,52]. Similarly, Lewatit MP 62 and Lewatit M 610 resins, containing tertiary amine functional groups, have been found to effectively adsorb Cr(VI) from water. Considering the need for efficient Cr(VI) removal from industrial wastewater, this study evaluates the adsorption potential of natural and modified diatomite, activated carbon, taurite, and the Lewatit M500 ion-exchange resin for the treatment of wastewater generated during ilmenite concentrate processing. The findings contribute to the development of cost-effective and sustainable sorbents for Cr(VI) removal, particularly in regions with abundant diatomite resources.

2. Materials and Methods

2.1. Experimental Methods

The processing of high-chromium ilmenite concentrate involves a series of operations, including preliminary reductive smelting, which facilitates the separation of iron into the magnetic fraction, while the non-magnetic fraction retains titanium oxides, chromium oxides, and other associated metal oxides. To convert trivalent chromium compounds (Cr(III)) into a water-soluble form, the non-magnetic fraction undergoes alkali roasting with sodium carbonate in an oxidizing atmosphere at 850 °C.

During this process, chromospinelide ($FeCr_2O_4$) is transformed into water-soluble sodium chromate (Na_2CrO_4). The roasted material is then leached with water, resulting in the dissolution of hexavalent chromium compounds (Cr(VI)) while titanium remains in the solid residue (cake).

For the experiments, aqueous solutions containing 4.5×10^3 and 6×10^3 mg/L of chromate ions were prepared by leaching the roasted (850 °C) non-magnetic titanium-containing fraction of the ilmenite concentrate with sodium carbonate.

2.2. Methods of Analysis

To conduct a comprehensive study of the investigated objects, advanced analytical techniques were employed, enabling an in-depth examination and understanding of their properties and behavior under various conditions. Elemental analysis of the initial materials and reaction products was conducted using the following analytical techniques: atomic absorption spectrometer AA-7000 (Shimadzu, Kyoto, Japan); inductively coupled plasma atomic emission spectrometer (ICP-AES) Optima 8300DV (PerkinElmer, Waltham, MA, USA); wavelength-dispersive X-ray fluorescence (WDXRF) spectrometer Venus 200 (MalvernPanalytical, Almelo, The Netherlands). The phase composition of the samples was determined using an X-ray diffractometer D8 Advance (Cu-Kα radiation, BRUKER AXS GmbH, Karlsruhe, Germany) with reference to the PDF-2 ICDD database (USA), under these specified parameters: 4–90° scan range, Cu–Kα radiation (λ = 0.15406 nm), tube voltage of 40 kV, tube current of 40 mA, and a continuous scanning speed of 1°/min. Microstructural and elemental composition analyses were performed using an electron probe microanalyzer JXA-8230 (JEOL, Tokyo, Japan). Infrared (IR) spectroscopy of the obtained products was carried out using a Fourier-transform infrared spectrometer (FTIR) FT/IR-6X (JASCO, Tokyo, Japan) in the spectral range of 4000–400 cm^{-1}. The KBr spectrum was recorded as a reference, and data processing was performed using Spectra Manager Ver.2.5 software. Potentiometric studies were conducted using a potentiometer pH200EM (InesaRex, Shanghai, China)

Activated carbon, taurite, and diatomite were ground using a grinder RM100 (Retsch, Düsseldorf, Germany) and sieved with a sieve C30/50 (Vibrotechnik, St. Petersburg,

Russia). For sorption studies, a reciprocating shaker SSL2 (Stuart, Stone, UK) was used for mixing and agitation of the solutions.

A BC-VP-4P vacuum pump (Value, Wenling, China) was used for the separation of the liquid phase and the washing of diatomite samples after their modification.

Chromium Ion Analysis in Initial and Post-Sorption Solutions Using Atomic Absorption Spectroscopy.

The determination of chromium ion concentrations in both the initial solutions and the solutions after the sorption process was carried out using an atomic absorption spectrometer (AA Shimadzu GmbH 7000, Kyoto, Japan). The atomic absorption spectrometry (AAS) method is based on measuring the resonance absorption of light by free chromium atoms at a wavelength of 357.9 nm. This occurs as the light passes through an atomic vapor formed during the electrothermal atomization of the water sample in the graphite furnace of the spectrometer.

Prior to analyzing the prepared wastewater samples, the spectrometer was calibrated using a standard solution series. The instrument's calibration curve was generated by plotting the arithmetic mean of measured atomic absorption values against the mass concentration of chromium ions, ensuring high accuracy in subsequent analyses.

To prepare the water samples for analysis, nitric acid was added as a background matrix at a ratio of 2 mL per 200 mL of the sample, followed by thorough mixing and conditioning for a minimum of 2 h. Before each measurement series, a blank sample containing chromium at a concentration not exceeding 0.001 mg/dm^3 was analyzed to verify the accuracy of the procedure. Aliquots of both the test samples and blank solutions were introduced into the graphite atomizer using an autosampler, and the absorption measurements were taken at 357.9 nm in duplicate to ensure reproducibility.

This method provides results with high metrological reliability, ensuring a confidence probability of p = 0.95 in accordance with GOST 31956-2012, the interstate standard for water analysis (GOST 31956-2012).

2.3. Materials Used in the Study

The following sorbents were tested for chromate ion removal from aqueous solutions: Activated carbon (BAU-A, manufacturer: Novochem, Kharkiv, Ukraine); taurite (Manufacturer: GRK "Koksu" LLP, Taldykorgan, Kazakhstan); natural diatomite from the Zhalpak deposit, Kandyagash, Kazakhstan); iron-modified diatomite (diatomite treated with iron salt solution); ion-exchange resin Lewatit MonoPlus M500—a strongly basic gel-type anion exchanger synthesized from a styrene-divinylbenzene copolymer (LEWATIT, manufacturer: LANX-ESS Deutschland GmbH, Koln, Germany). Additionally, the following reagents were used: ferric chloride ($FeCl_3$) (purity $\geq$ 96%, CAS No.: 7705-08-0, manufacturer: Shandong Yili-Spring Chemical Industry Co., Ltd., Zouping, China); sodium hydroxide (NaOH) (analytical grade, P.A.—99.9%, GOST 4328-77, manufacturer: JSC "Kaustik", Pavlodar, Kazakhstan). Sulfuric acid (98.5% H_2SO_4), ACS reagent, 95.0–98.0%, utilized without additional purification, was obtained from Merck Sigma-Aldrich, Almaty, Kazakhstan. Ultrapure water (18.2 MΩ·cm) was employed for the preparation of all solutions.

In this study, the initial diatomite raw material was first crushed and ground to break down larger aggregates into smaller particles, followed by sieving to obtain fractions of 0.5, 1.0, 2.0, 3.2, 4.0, and 8.0 mm. The selection of appropriate fractions is crucial for optimizing performance in sorption, filtration, and catalytic processes. Based on preliminary assessments, the 0.5 mm and 2.0 mm fractions were chosen for further investigation due to their structural characteristics and potential for enhanced adsorption performance. The subsequent sections present a detailed analysis of their chemical composition, phase structure, and other relevant properties.

To improve the adsorption efficiency of diatomite, a chemical modification process was employed by precipitating iron hydroxide onto its surface from solution. The natural diatomite was treated with a 50% solution mixture of $FeCl_3$ and NaOH in accordance with the stoichiometry of their interaction reaction. The modification process was conducted at room temperature for 12 h under continuous stirring to ensure uniform deposition of iron hydroxide on the diatomite surface. Following the reaction, the liquid phase was separated using a Büchner funnel, a Büchner flask, and a vacuum pump. Finally, the modified diatomite was dried at 105 °C until a constant weight was achieved.

The activated carbon samples were first washed thoroughly with distilled water to remove any surface impurities. The material was then dried at 100 °C for 24 h to eliminate residual moisture. After drying, the samples were ground using a laboratory mill and sieved to achieve a uniform particle size distribution. To further enhance the carbon structure and optimize adsorption properties, the activated carbon underwent carbonization at 550 °C for 25 min. After thermal treatment, the carbonized material was sieved again to ensure particle size consistency for subsequent adsorption studies.

Taurite, a processed derivative of natural shungite raw material obtained from the Koksu deposit in Kazakhstan, was prepared through a series of processing steps. Initially, it was washed with deionized water to remove dust and fine particles. The material was then dried in an oven at 105 °C until a constant mass was achieved. To ensure uniformity, taurite was ground using a grinder to a particle size of 2.0 mm. The ground material was then sieved through a mesh of the appropriate pore size to obtain a homogeneous fraction. The prepared taurite was stored in airtight containers to prevent contamination and moisture absorption from the ambient air.

2.4. Preparation of Lewatit MonoPlus M500 for Sorption Studies

The preparation of Lewatit MonoPlus M500 ion-exchange resin for sorption experiments was conducted as follows:

The resin was thoroughly washed with deionized water to remove dust and fine particles, preventing contamination and enhancing sorption efficiency. The resin was regenerated using a sodium hydroxide (NaOH) solution to activate its functional groups and improve sorption performance. After regeneration, the resin was rinsed with deionized water to eliminate residual regeneration solution. A working solution with the required concentration and pH was prepared for sorption experiments, ensuring that it met specific experimental requirements. The prepared resin was introduced into the reaction vessel designated for static sorption, ensuring even distribution and the absence of air pockets. For resin regeneration, a sodium hydroxide solution with a concentration of 1–2 M was used, depending on the specific research conditions and manufacturer recommendations. The preparation of NaOH solutions followed these guidelines:

1. M NaOH Solution: 40 g of NaOH dissolved in 1 L of deionized water.
2. M NaOH Solution: 80 g of NaOH dissolved in 1 L of deionized water.

2.5. Adsorption Experiments

All adsorption experiments were conducted at a constant temperature of 25 °C with continuous shaking at 200 rpm. A 50 mL stock solution containing hexavalent chromium ions was introduced into a 250 mL Erlenmeyer flask along with a sorbent dosage of 5×10^3 mg. The adsorption process was conducted over 24 h to ensure equilibrium. To maintain a stable temperature, the flask was placed in an air thermostat. After the designated contact time, the suspension was filtered using filter paper, and the adsorption efficiency was analyzed by determining the residual concentration of chromium ions in the filtrate.

2.6. Industrial Effluent Treatment Process

The industrial effluent utilized in this study originated from the processing of leucoxene–ilmenite concentrate from the Obukhovskoe deposit in Kazakhstan. The extraction of Cr(VI)-containing aqueous waste involved the following key steps:

Oxidative roasting: Ilmenite concentrate was roasted at 900–1100 °C with and without 4% and 6% calcined soda, promoting Fe(II) oxidation to Fe(III) oxides and forming water-soluble chromates.

Reduction roasting: The oxidized material was treated under an argon atmosphere at 1000 °C to enhance selective separation of iron and chromium phases.

Smelting and phase separation: High-temperature smelting (1600–1700 °C) enabled the separation of metallic iron and chromium, concentrating titanium and rare-earth elements in the slag.

Slag milling and leaching: The titanium-rich slag was ground (0.044 mm), sintered with sodium carbonate (950 °C), and leached in hot water (80 °C, 30 min) for chromium extraction.

This stepwise process ensured the effective removal of chromium from the ilmenite concentrate while generating a Cr(VI)-containing industrial effluent suitable for subsequent sorption studies. The methodology ensuring a controlled approach to managing chromium contamination during titanium processing while also facilitating the recovery of valuable elements as described in [15].

3. Results and Discussion

In the present study, a comprehensive analysis of diatomite samples was conducted to evaluate their structural and compositional characteristics. Particular emphasis was placed on different particle size fractions, as variations in grain size can significantly influence material properties, including porosity, surface reactivity, and sorption capacity. The chemical and phase compositions of two diatomite fractions (0.5 mm and 2.0 mm) were examined to assess their suitability for further modification and application.

The elemental composition of diatomite was analyzed for different particle size fractions. The 0.5 mm fraction was found to consist of the following components: silicon dioxide (SiO_2), aluminum oxide (Al_2O_3), iron (III) oxide (Fe_2O_3), titanium dioxide (TiO_2), sodium oxide (Na_2O), magnesium oxide (MgO), and calcium oxide (CaO). Similarly, for the 2.0 mm fraction, the composition included SiO_2, Al_2O_3, Fe_2O_3, TiO_2, Na_2O, MgO, and CaO. Overall, diatomite was found to be predominantly composed of silicon dioxide, with aluminum oxide, iron (III) oxide, titanium dioxide, sodium oxide, magnesium oxide, and calcium oxide present as minor constituents. These components are likely associated with clay minerals, feldspars, and carbonate impurities, which naturally occur in diatomaceous deposits and contribute to the material's physicochemical properties.

Table 1 presents the elemental composition of diatomite for different particle size fractions. The 0.5 mm fraction was found to contain 69.45% SiO_2, 8.12% Al_2O_3, 3.19% Fe_2O_3, 1.03% TiO_2, 0.98% Na_2O, 0.94% MgO, and 0.75% CaO. In comparison, the 2.0 mm fraction exhibited a higher silica content (75.67% SiO_2) and a lower calcium oxide concentration (0.42% CaO), indicating variations in mineral distribution across different particle sizes.

The results of X-ray phase analysis for diatomite fractions of 0.5 mm and 2.0 mm are presented in Figures 1 and 2. The main phase of diatomite is quartz SiO_2—52.7%; the other minerals are kaolinite $Al_2[Si_2O_5](OH)_4$—17%; muscovite $KAl_2[AlSi_3O_{10}](OH)_2$—13.2%; sodium aluminosilicate (paragonite) $NaAl_2(AlSi_3)O_{11}$)—7.5%; halite NaCl—5.9%; palygorskite $Mg_5(Si_4O_{10})_2(OH)_2(H_2O)_8$—3.9%.

Table 1. Elemental composition of diatomite for different particle size fractions (%).

No.	Component	0.5 mm Fraction (%)	2.0 mm Fraction (%)
1	SiO_2	69.45	75.67
2	Al_2O_3	8.12	8.77
3	Fe_2O_3	3.19	3.21
4	TiO_2	1.03	1.23
5	Na_2O	0.98	1.09
6	MgO	0.94	1.03

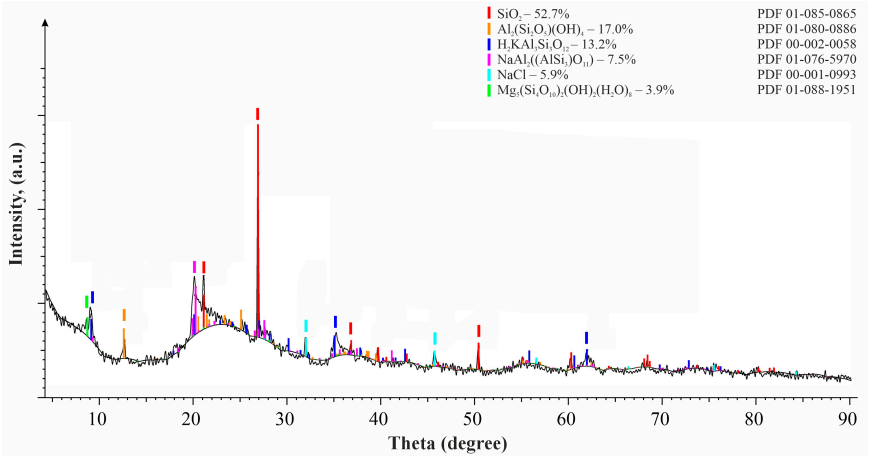


Figure 1. X-ray diffraction of natural diatomite (0.5 mm fraction).

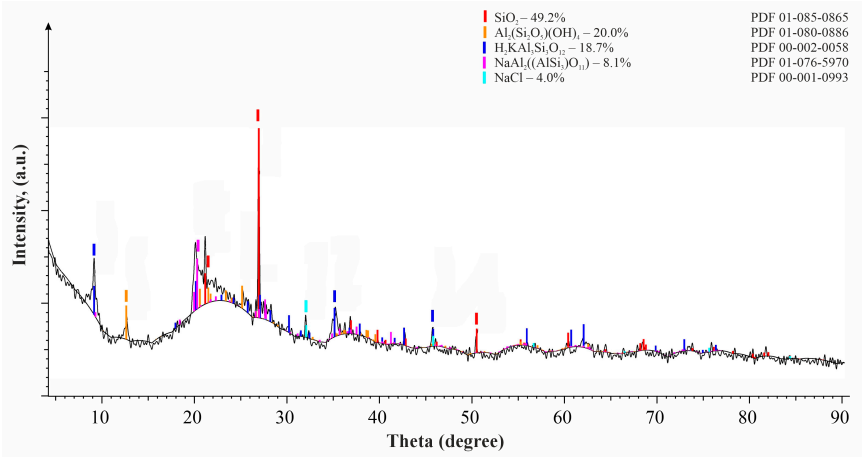


Figure 2. X-ray diffraction of natural diatomite (2.0 mm fraction).

A sample of a larger fraction of diatomite (2.0 mm) has a similar composition: quartz—49.2%; kaolinite—20%; sodium aluminosilicate—8.1%; halite NaCl—4.0%; and the muscovite content increases to 18.7%.

The analysis of various diatomite fractions revealed that they exhibit no significant differences in their chemical and phase composition. In subsequent experiments, the 2.0 mm diatomite fraction was selected due to its superior physico-mechanical properties. The results of the electron microscopic study of the 2.0 mm diatomite fractions are shown in Figures 3 and 4. SEM images of the studied samples show the classical microstructure of diatomite, including globules, valves, and flaps having cylindrical, linear, and disc-shaped forms, as well as clastic fragments of clay minerals (Figure 3).

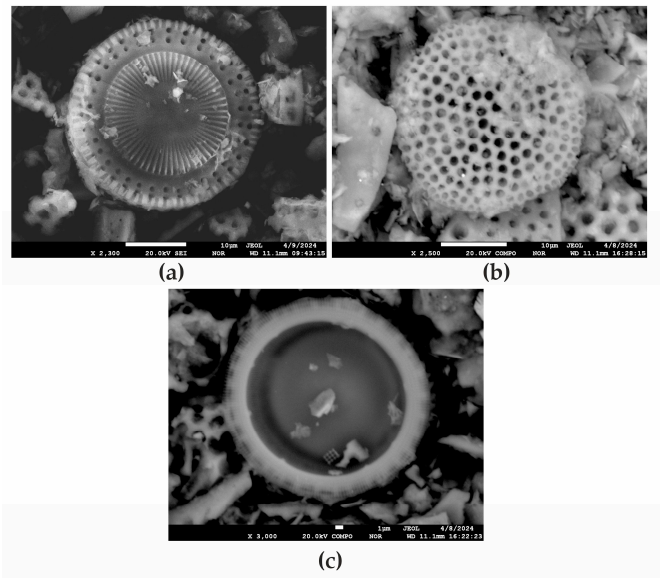


Figure 3. SEM images of structural elements of natural diatomaceous earth: ×2300 (**a**), ×2500 (**b**), and ×3000 (**c**).

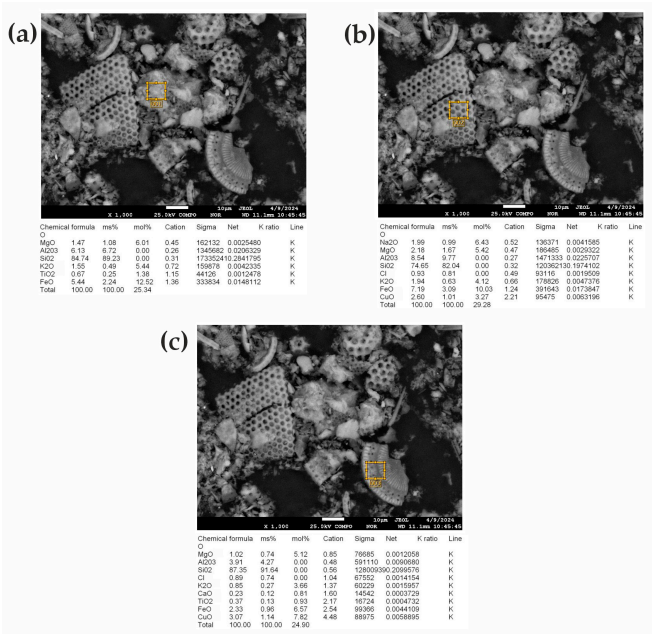


Figure 4. SEM images of a natural diatomite sample with a particle thickness of 2.0 mm, accompanied by point elemental analysis of diatoms exhibiting radial symmetry: a fragment of a honeycomb-like diatom frustule (**a**), a complete honeycomb-structured frustule (**b**), and a centric-type diatom frustule (**c**) (×1000).

Table 2 presents the elemental compositions of individual regions of diatomite structural elements. The results indicate that silicon dioxide dominates the composition, with aluminum oxide, iron oxide, and magnesium oxide present in appreciable amounts (Figure 4).

The changes introduced by this modification were further confirmed through infrared spectroscopy analysis. The FTIR spectra indicated the formation of iron oxyhydroxide (FeO(OH)), as evidenced by the characteristic absorption bands at 3401.82 cm^{-1} and 3459.67 cm^{-1} (Figure 5). Additionally, the spectra revealed absorption bands corresponding to quartz (SiO_2) at 797.42, 777.17, and 466.69 cm^{-1} and paragonite ($NaAl_2(AlSi_3O_{10})(OH)_2$) at 993.16, 733.78, 710.64, and 670.14 cm^{-1}. The presence of clay minerals was also identified, including kaolinite ($Al_2Si_2O_5(OH)_4$), with bands at 3693.01, 1644.02, 922.77, and

437.76 cm^{-1} and palygorskite ($Na(MgAl)_2[Si_4O_{10}](OH)2{\cdot}4H_2O$), at 922.77, 850.45, and 466.69 cm^{-1}. Additionally, aluminum oxide (Al_2O_3) was detected at 596.86 cm^{-1}.

Table 2. Elemental compositions of diatomite structural elements (%).

Component	Region 1 (%), Figure 4a	Region 2 (%), Figure 4b	Region 3 (%), Figure 4c
SiO_2	89.23	82.04	91.64
Al_2O_3	6.72	9.77	4.27
FeO	2.24	3.09	0.96
MgO	1.08	1.67	0.74

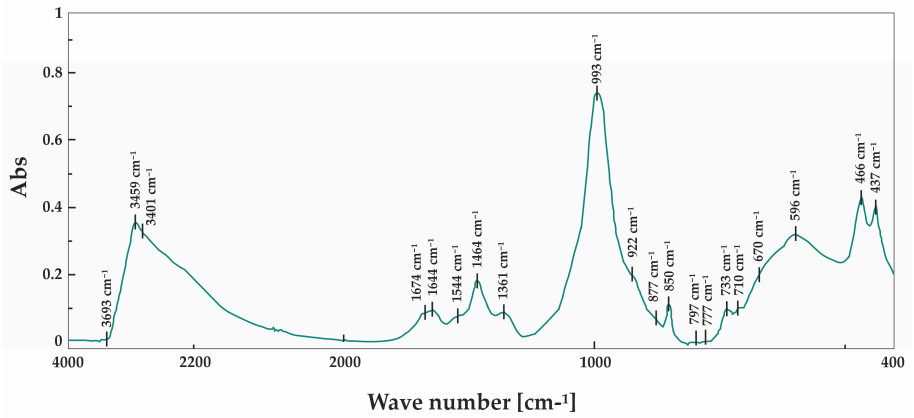


Figure 5. Infrared spectrum of modified diatomite sample.

To further evaluate the impact of modification, the surface morphologies and elemental compositions were analyzed using scanning electron microscopy (SEM) (Figure 6). The chemical composition of natural diatomite before and after modification is presented in Table 3. Unmodified diatomite exhibited a highly porous structure, primarily composed of silicon dioxide (41.79 wt%), aluminum oxide (6.18 wt%), and iron oxide (1.00 wt%). Following modification, the diatomite surface became covered with irregularly shaped iron-rich deposits, leading to a significant increase in iron content (39.17 wt% Fe_2O_3) accompanied by a notable decrease in silicon dioxide (3.17 wt% SiO_2) and aluminum oxide (0.60 wt% Al_2O_3).

Table 3. Surface composition of natural and modified diatomite (wt%).

Component	Natural Diatomite, wt% (Figure 6a)	Modified Diatomite, wt% (Figure 6b)	Post-Washing, wt% (Figure 6c)
SiO_2	41.79	3.17	45.39
Al_2O_3	6.18	0.60	6.71
Fe_2O_3	1.00	39.17	1.93

After post-sorption washing, the chemical composition nearly returned to its initial state. These results confirm the successful modification of diatomite through iron oxyhydroxide precipitation and demonstrate its ability to regenerate following the sorption process. This highlights its potential as a reusable adsorbent for Cr(VI) removal.

To investigate the influence of key parameters such as contact time (0–300 min), pH level (1–7), adsorbent dosage (0.2–5 g/L), and adsorbate concentration (4–6 g/L) on the sorption process of Cr(VI) from aqueous solutions using activated carbon, a series of batch

sorption experiments was conducted. All adsorption studies were performed at room temperature (25 °C) under vigorous stirring (200 rpm) using 50 mL of Cr(VI) solution placed in a 250 mL Erlenmeyer flask. Upon completion of the adsorption process, the flask contents were filtered. Each experiment was conducted in duplicate, and the averaged values were used for analysis.

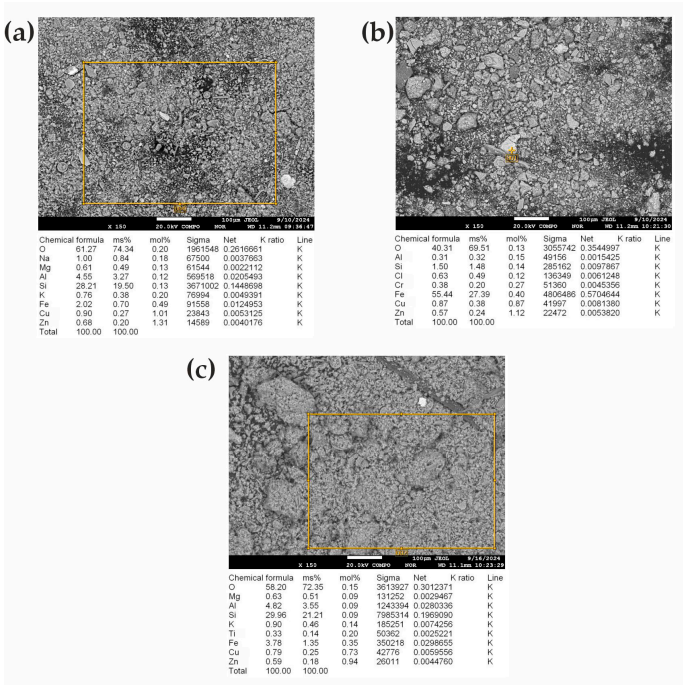


Figure 6. SEM images of samples of natural diatomite (**a**), modified diatomite (**b**), and diatomite after washing (**c**) (×150).

The acidity of the solution significantly influenced the sorption activity of the adsorbent toward chromium ions. To examine the effect of pH on Cr(VI) sorption, a series of batch experiments was performed under static conditions using acetate–ammonium buffer solutions at varying pH levels. The pH of the tested solutions was continuously monitored using a pH meter. The solutions were stirred, and at predetermined intervals, aliquots were collected to determine the residual Cr(VI) concentration. The pH range studied varied from 1 to 7, with the highest Cr(VI) sorption observed at pH 1 and 2. The time-dependent Cr(VI) adsorption process was examined over 7 h. Adsorbent samples of 0.2, 0.3, 0.5, 0.75, 1, and 2 g were introduced into 100 mL of metal-containing solution with an initial Cr(VI) concentration of 0.2 g/L. The solutions were stirred, and Cr(VI) concentrations were measured at regular time intervals. Additionally, the adsorption behavior of chromate ions on both natural and Fe-modified diatomite was investigated as a function of contact time (0–300 min), pH level (1–7), adsorbent dosage (0.2×10^3–5.0×10^3 mg/L), and adsorbate concentration (0.9×10^3–6.0×10^3 mg/L). The research findings are presented in Figure 7.

The data analysis indicates that chromate ions ($Cr_2O_7^{2-}$) exhibit the highest adsorption efficiency in an acidic medium for both natural and modified diatomite. The sorption process, encompassing both adsorption and desorption stages, was systematically examined using Lewatit MonoPlus M500, natural and modified diatomite, taurite, and activated carbon. The experiments were performed under static conditions with periodic stirring, ensuring that equilibrium was reached within the studied systems. The chromium concentration in the solutions was analyzed to assess the sorption capacity of each sorbent. To investigate desorption behavior, chromium-saturated sorbents were treated with sodium hydroxide (NaOH) solutions in systems with pH 1.5 or sulfuric acid (H_2SO_4) solutions in

systems with pH 13.5, using different molar concentrations (0.05 M, 1 M, and 2 M). The desorption efficiency was quantified by measuring the amount of chromium ions released back into the solution (Table 1). The chromate ion removal efficiency was calculated using the following formula:

$$\eta = (C_0 - C_e)/C_0 \times 100\%, \quad (1)$$

where C_0 is the initial starting concentration of chromate ions in the solution, mg/L; and C_e is the residual concentration of chromate ions in the solution, mg/L.

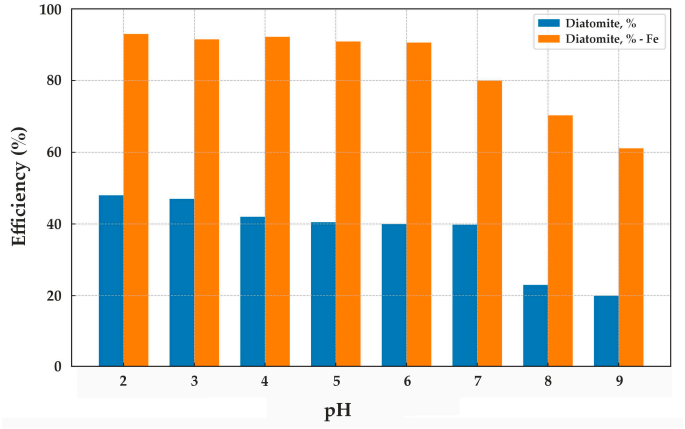


Figure 7. Effect of pH on the adsorption of chromate ions onto natural and modified diatomite.

Tables 4–6 present the sorption and desorption data for Cr(VI) ions from solution using Lewatit MonoPlus M500, natural diatomite, modified diatomite, taurite (shungite), and activated carbon.

Figure 8 presents a diagram illustrating the sorption extraction rates of chromate ions at various Cr(VI) ion concentrations (C_{01} = 994, C_{02} = 1998, C_{03} = 2982, C_{04} = 3976, and C_{05} = 4970 mg/L) in solution for the five investigated sorbents: natural diatomite, modified diatomite, taurite, activated carbon, and Lewatit MonoPlus M500.

Figure 9 presents the chromate ion desorption diagram for the five studied sorbents: natural diatomite, modified diatomite, taurite (shungite), activated carbon, and Lewatit MonoPlus M500.

A series of sorption experiments for Cr(VI) ions demonstrated that activated carbon and natural diatomite exhibit low sorption capacities, whereas Fe-modified diatomite and Lewatit MonoPlus 500 exhibit high sorption efficiency. Consequently, further investigations were focused on Fe-modified diatomite and Lewatit MonoPlus 500.

Table 4. Sorption and desorption data of Cr(VI) ions from solution onto natural and modified diatomite.

No.	C_{00}, mg/L	Sorption Efficiency η for Modified Diatomite, %	Desorption of Cr(VI) from Modified Diatomite, %	Sorption Efficiency η for Natural Diatomite, %	Desorption of Cr(VI) from Natural Diatomite, %
1	C_{01} = 0.994	98.990	92.91	49.445	91.55
2	C_{02} = 1.998	98.998	92.99	49.395	92.00
3	C_{03} = 2.982	98.993	93.05	49.279	91.73
4	C_{04} = 3.976	98.993	92.84	49.144	91.84
5	C_{05} = 4.970	98.792	93.77	48.993	92.05

where C_{00} (mg/L)—Initial concentration of Cr(VI) ions in solution; sorption efficiency, η (%)—percentage of Cr(VI) ions adsorbed onto natural and modified diatomite; desorption of Cr(VI) (%)—percentage of Cr(VI) ions desorbed from natural and modified diatomite.

Table 5. Sorption and desorption data of Cr(VI) ions from solution onto Lewatit MonoPlus M500.

No.	C_{00}, mg/L	Sorption Efficiency η onto Lewatit M500, %	Desorption of Cr(VI) from Lewatit M500, %
1	C_{01} = 994	98.692	98.68
2	C_{02} = 1998	98.698	98.77
3	C_{03} = 2982	98.423	97.97
4	C_{04} = 3976	98.138	98.25
5	C_{05} = 4970	97.786	98.91

where C_{00} (mg/L)—initial concentration of Cr(VI) ions in solution; sorption efficiency, η (%)—percentage of Cr(VI) ions adsorbed onto Lewatit M500; desorption of Cr(VI) (%)—percentage of Cr(VI) ions desorbed from Lewatit M500.

Table 6. Sorption and desorption data of Cr(VI) ions from solution onto taurite (shungite) and activated carbon.

No.	C_{00}, mg/L	Sorption Efficiency η onto Taurite, %	Desorption of Cr(VI) from Taurite, %	Sorption Efficiency η onto Activated Carbon, %	Desorption of Cr(VI) from Activated Carbon, %
1	C_{01} = 994	72.21	80.21	75.16	85.16
2	C_{02} = 1998	72.45	81.12	75.14	85.60
3	C_{03} = 2982	72.20	83.00	75.12	84.88
4	C_{04} = 3976	72.39	81.88	74.30	84.65
5	C_{05} = 4970	72.40	82.30	75.09	85.25

where: C_{00} (mg/L)—initial concentration of Cr(VI) ions in solution; sorption efficiency, η (%)—percentage of Cr(VI) ions adsorbed onto taurite and activated carbon; desorption of Cr(VI) (%)—percentage of Cr(VI) ions desorbed from taurite and activated carbon.

Based on the observed chromium concentration decrease within the pH range of 2 to 4, pH 4 was identified as the optimal condition for determining adsorption isotherms. Experimental results indicate that adsorption time significantly affects Cr(VI) removal efficiency.

For natural diatomite, the maximum chromate ion removal was achieved within 120 min, whereas Fe-modified diatomite reached adsorption equilibrium within 60 min. To gain deeper insights into the sorption process of hexavalent chromium ions on the investigated sorbents, mathematical modeling of the experimental data was performed. The adsorption characteristics of the studied systems were evaluated using the Langmuir, Freundlich, and Dubinin–Radushkevich isotherm models, each representing different sorption mechanisms. The Langmuir isotherm describes monolayer adsorption on a homogeneous surface, assuming that all sorption sites are identical. The Freundlich isotherm characterizes multilayer adsorption on a heterogeneous surface with variable energy sorption sites. The Dubinin–Radushkevich isotherm is used to describe adsorption in micropores, which is particularly relevant for porous materials such as diatomite. The experimental data were best fitted to the Langmuir model, allowing for the determination of the maximum sorption capacity (q_{max}) and the adsorption equilibrium constant (b). The linearized form of the Langmuir equation was utilized to estimate these parameters.

$$\frac{C_e}{q_e} = \frac{1}{q_{max} b} + \frac{C_e}{q_{max}} \quad (2)$$

where b is the adsorption equilibrium constant, representing the interaction energy between the adsorbent and adsorbate, and q_{max} corresponds to the saturation capacity of the monolayer.

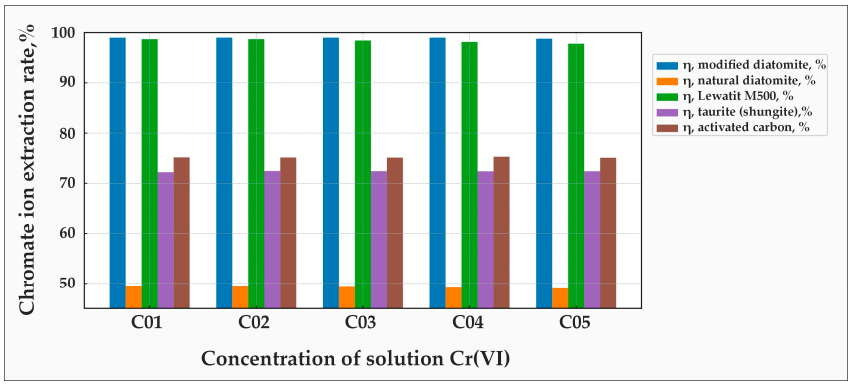


Figure 8. Sorption rate of chromate ions onto Lewatit MonoPlus M500, natural and modified diatomite, taurite (shungite), and activated carbon.

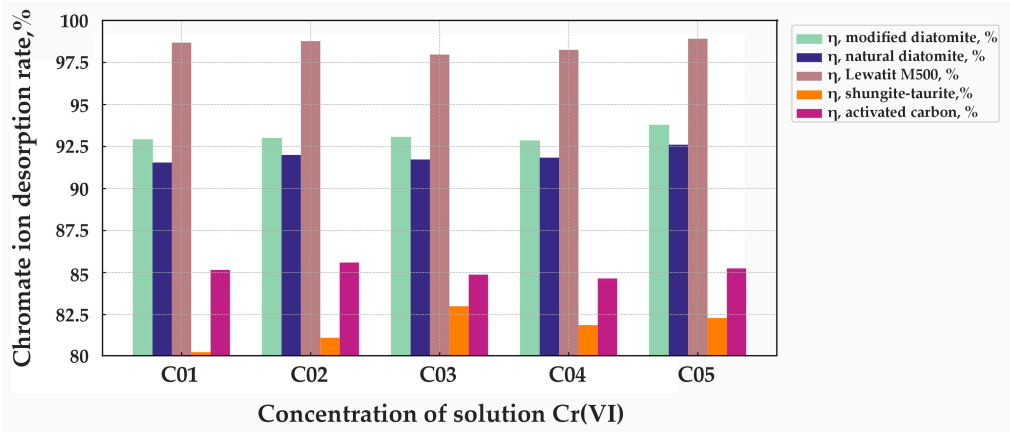


Figure 9. Comparative diagram of chromate ion desorption from natural diatomite, modified diatomite, shungite-taurite, activated carbon, and Lewatit MonoPlus M500.

Since real adsorbent surfaces exhibit geometric heterogeneity, the adsorption process was also analyzed using the Freundlich model, which is suitable for heterogeneous surfaces. The linear form of the Freundlich equation was used to determine the Freundlich adsorption constant (K_f) and intensity parameter ($1/n$):

$$\log q_e = \log K_f + \frac{1}{n}\log C_e \quad (3)$$

where K_f represents the adsorption capacity and n is related to adsorption intensity and surface heterogeneity. The Freundlich model assumes an exponential distribution of adsorption site energies, meaning that the probability of high-energy sites decreases as energy increases.

Comparative analysis of the adsorption behavior of Lewatit MonoPlus M500, natural diatomite, and Fe-modified diatomite confirmed that the Langmuir model best described Cr(VI) adsorption for Lewatit MonoPlus M500 and Fe-modified diatomite, indicating monolayer coverage of sorption sites. In contrast, natural diatomite exhibited a better fit to the Freundlich model, suggesting multilayer adsorption due to surface heterogeneity. For the construction of adsorption isotherms, necessary mathematical calculations were performed based on the results of the chemical analysis of solutions used for the sorption of chromate ions from model solutions. The data are presented in Tables 7 and 8.

Table 7. Sorption of chromate ions onto Lewatit MonoPlus M500.

C_0, mg/L	C_e, mg/L	$V_{filtrate}$, L	$m_{sorbent}$, mg	q_e, mg/g
994	13	0.05	5000	9.81
1998	26	0.05	5000	19.72
2982	47	0.05	5000	29.35
3976	74	0.05	5000	39.02
4970	110	0.05	5000	48.60

where C_0 (mg/L)—initial concentration of Cr(VI) ions in solution; C_e (mg/L)—equilibrium concentration of Cr(VI) ions in solution after sorption; $V_{filtrate}$ (L)—volume of the filtrate solution; $m_{sorbent}$ (mg)—mass of the sorbent used in the experiment; q_e (mg/g)—equilibrium sorption capacity of the sorbent.

Table 8. Langmuir isotherm data for the sorption onto Lewatit MonoPlus M500.

q_e, mg/g	C_e, mg/L	C_e/q_e
9.81	13	1.325178389
19.72	26	1.318458418
29.35	47	1.601362862
39.02	74	1.896463352
48.6	110	2.263374486
q_{max}, mg/g	b, L/mg	R_L
97.08737864	0.01159368	0.028
		0.028111719

where q_e (mg/g)—equilibrium sorption capacity of the sorbent; C_e (mg/L)—equilibrium concentration of Cr(VI) ions in solution; C_e/q_e (L/g)—ratio of equilibrium concentration to equilibrium sorption capacity, used for Langmuir isotherm calculations; q_{max} (mg/g)—maximum sorption capacity of the sorbent, as determined by the Langmuir isotherm; b (L/mg)—Langmuir constant related to the affinity between the sorbate and the sorbent; R_L—dimensionless separation factor, indicating the favorability of the adsorption process.

The Langmuir isotherm equation for Lewatit MonoPlus M500 in this study is given as follows:

$$y = 0.0103x + 1.1256 \quad (4)$$

with a determination coefficient of R^2 value = 0.9845 (Figure 10).

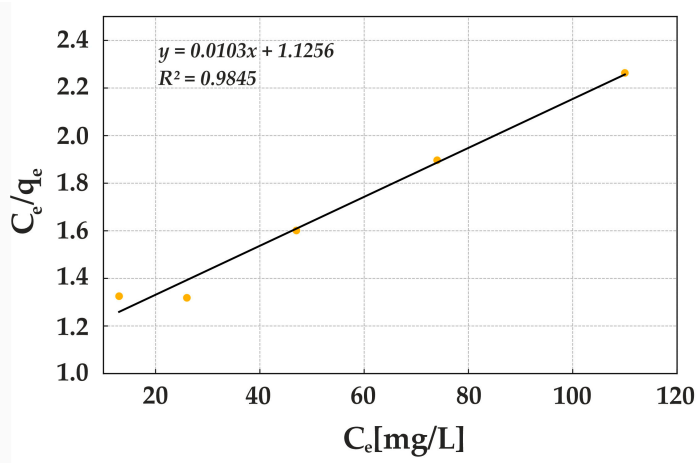


Figure 10. Langmuir isotherm for the sorption onto Lewatit MonoPlus M500.

The slope coefficient, 0.0103, represents the reciprocal of the sorption capacity and is associated with the saturation of sorption sites. A lower value indicates a relatively low sorbent capacity for the adsorbate and suggests that the sorption process slows down as the sorbent becomes saturated. The intercept, 1.1256, is related to the Langmuir constant and reflects the interaction strength between the sorbent and the Cr(VI) ions. A value greater than one indicates a relatively strong interaction between the anion and the anion exchanger. The determination coefficient R^2 = 0.9845 suggests a strong fit of the experimental data to the Langmuir model, confirming that sorption on this sorbent follows a monolayer adsorption mechanism. Based on these findings, the adsorption process in this system is predictable and well described by the Langmuir equation.

In the case of sorption using natural and modified diatomite, mathematical calculations and the data from sorption studies presented in Tables 9–12 were used to determine Langmuir isotherms and derive the corresponding linear equations.

Table 9. Chromate ion Cr(VI) sorption results for natural diatomite.

C_o, mg/L	C_e, mg/L	$V_{filtrate}$, L	$m_{sorbent}$, mg	q_e, mg/g
994	18	0.05	5000	9.76
1998	40	0.05	5000	19.58
2982	52	0.05	5000	29.30
3976	80	0.05	5000	38.96
4970	100	0.05	5000	48.70

where: C_0 (mg/L)—initial concentration of Cr(VI) ions in solution; C_e (mg/L)—equilibrium con-centration of Cr(VI) ions in solution after sorption.

Table 10. Data for the construction of the Langmuir isotherm for sorption onto natural diatomite.

q_e, mg/g	C_e, mg/L	C_e/q_e
9.76	18	1.844262295
19.58	40	2.42900919
29.3	52	1.774744027
38.96	80	2.05338809
48.7	100	2.05338809
q_{max}, mg/g	b, L/mg	R_L
416.6666667	0.00435072	0.072
		0.071562255

where: C_e (mg/L)—equilibrium con-centration of Cr(VI) ions in solution after sorption.

Table 11. Results of chromate ion sorption onto modified diatomite.

C_o, mg/L	C_e, mg/L	$V_{filtrate}$, L	$m_{sorbent}$, mg	q_e, mg/g
994	10	0.05	5000	9.84
1998	20	0.05	5000	19.78
2982	30	0.05	5000	29.52
3976	40	0.05	5000	39.36
4970	60	0.05	5000	49.10

Table 12. Data for the Langmuir isotherm for sorption onto modified diatomite.

q_e, mg/g	C_e, mg/L	C_e/q_e
9.84	10	1.016260163
19.78	20	1.011122346
29.52	30	1.016260163
39.36	40	1.016260163
49.10	60	1.221995927
q_{max}, mg/g	b, L/mg	R_L
99.00990099	0.01136856	0.028
		0.028652436

Two linear equations were obtained:

1. for natural diatomite:

$$y = 0.001x + 101.43;\ R^2 = 0.9888 \quad (5)$$

2. for modified diatomite:

$$y = 0.0039x + 0.9305;\ R^2 = 0.6677 \quad (6)$$

The Langmuir isotherm for natural diatomite (Figure 11) characterizes a monomolecular type of adsorption on a homogeneous surface. The determination coefficient $R^2 = 0.9888$ indicates a strong correlation between the data and the Langmuir model. The maximum adsorption capacity q_{max}, calculated from the slope of the Langmuir isotherm, is . This relatively low value compared with other adsorbents such as activated carbon, synthetic zeolites, or functionalized materials, which often exhibit $q_{max} > 100$ mg/g for Cr(VI), suggests limited adsorption potential.

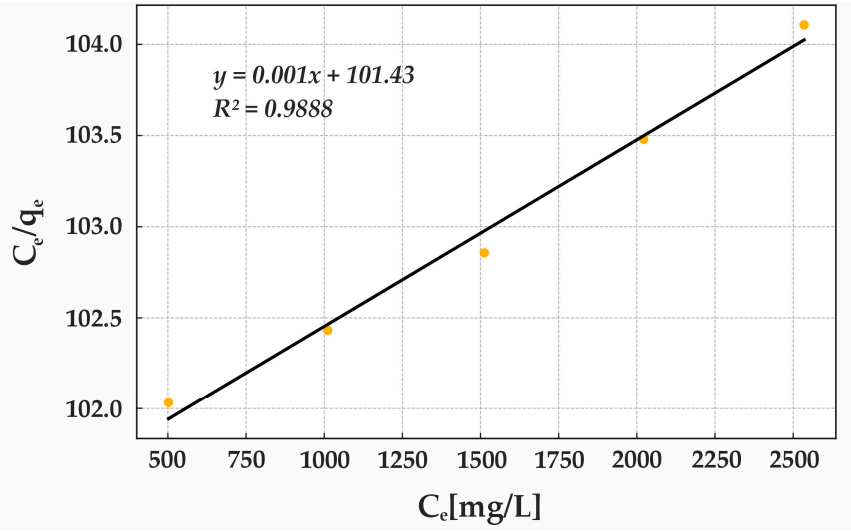


Figure 11. Langmuir isotherm for sorption onto natural diatomite.

The low adsorption capacity can be attributed to the natural properties of diatomite, including its high silica content, which has limited sorption properties due to the absence of strong active sites for Cr(VI) binding. Additionally, the low surface area and porosity of natural diatomite compared with modified adsorbents further limit its performance. The lack of modification also reduces its sorption capacity, as unmodified diatomite lacks specific functional groups (e.g., amine groups or metal complexes) that could enhance its

affinity for Cr(VI). The adsorption equilibrium constant further indicates weak interaction between the adsorbate (Cr(VI)) and natural diatomite.

For modified diatomite (Figure 12), the slope coefficient, which is inversely related to the maximum adsorption capacity, is approximately 256.41 mg/g. This result demonstrates a significantly enhanced adsorption capacity compared with natural, unmodified diatomite. The modification process likely introduced additional active sites, leading to a stronger interaction between the adsorbent and Cr(VI) ions. However, the determination coefficient R^2 = 0.6677 is lower than that of natural diatomite, indicating that the Langmuir model does not perfectly describe the adsorption process on modified diatomite.

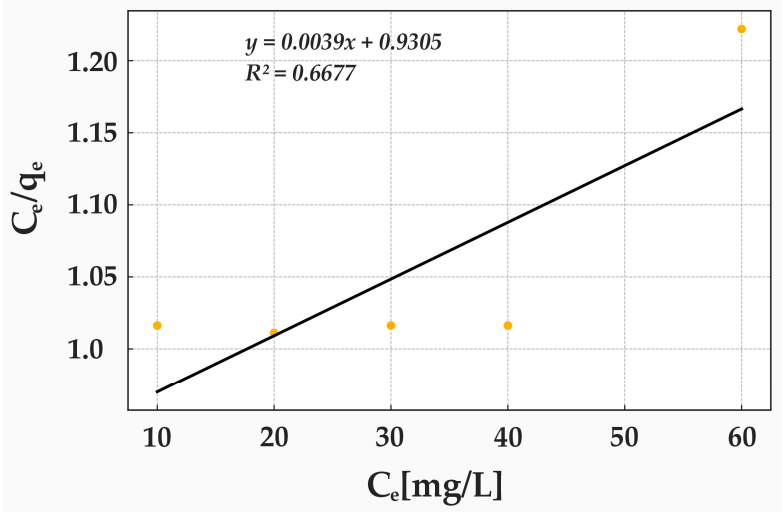


Figure 12. Langmuir isotherm for sorption onto modified diatomite.

Despite the informativeness of Langmuir isotherms for describing the sorption processes involving natural and modified diatomite, the low R^2 = 0.6677 value indicates a poor fit between the experimental data and the linear model. Since values closer to 1 indicate better explanatory power, the relatively low R^2 suggests that the Langmuir equation does not fully describe the experimental results. A different model or a more complex isotherm may be more suitable for this system.

The Freundlich isotherm parameters were calculated for Lewatit MonoPlus M500, natural diatomite, and modified diatomite. The parameters outlined in (Table 13) detail the sorption properties of these materials. The Freundlich isotherm for Lewatit MonoPlus M500 (Figure 13) indicates the presence of heterogeneous sorption sites and the ability of the sorbent to facilitate multilayer adsorption. Some active sites exhibit stronger interactions with anions than others, resulting in a gradual decrease in sorption efficiency as the adsorbate concentration increases.

Table 13. Calculation parameters for the construction of the Freundlich isotherm.

Equation	C_0, mg/L	C_0, mg/L	R^2	K_f	n
Lewatit M500	y = 1.3297x − 0.2478	994	0.9843	0.565	0.75205
Natural diatomite	y = 1.012x + 1.9995	994	1	99.88	0.98814
Modified diatomite	y = 1.0752x − 0.0833	994	0.9902	0.929	0.93006

While the Langmuir isotherm for Lewatit MonoPlus M500 suggested predominantly monomolecular adsorption with strong adsorbate–sorbent interactions, the Freundlich isotherm demonstrates the presence of heterogeneous sorption sites. This variation allows

the sorbent to maintain high-efficiency sorption across different adsorbate concentrations by combining high-energy active sites with regions of lower sorption energy.

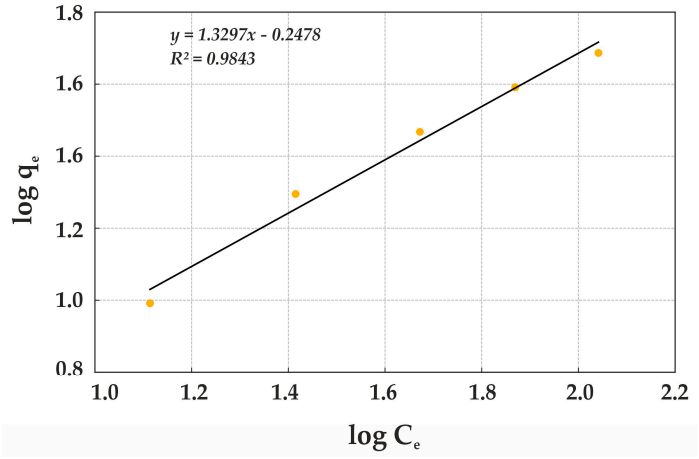


Figure 13. Freundlich adsorption isotherm for the sorption onto Lewatit MonoPlus M500.

The Freundlich isotherm for natural diatomite (Figure 14) indicates that this sorbent effectively absorbs Cr(VI) at low concentrations; however, its adsorption capacity gradually decreases as the sorbent becomes saturated. This behavior aligns well with the Freundlich model, demonstrating that diatomite can serve as a viable adsorbent for water treatment, though modified forms of natural diatomite exhibit higher efficiency in Cr(VI) removal.

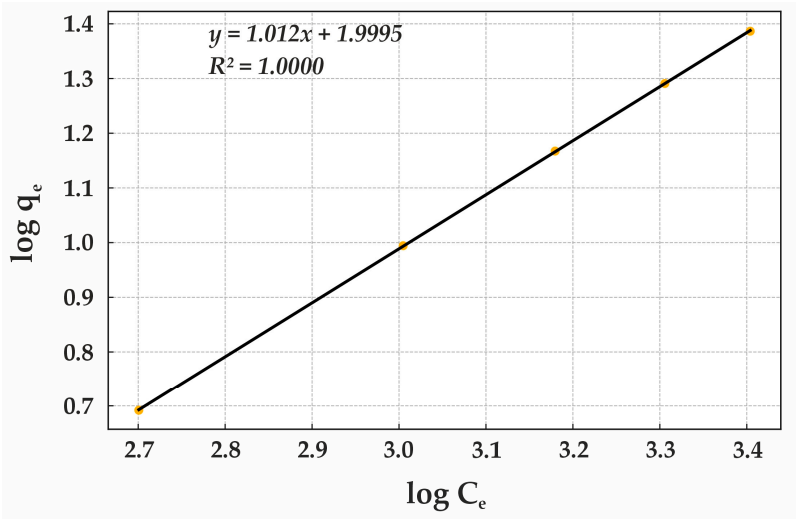


Figure 14. Freundlich adsorption isotherm for sorption onto natural diatomite.

Modified diatomite exhibits significantly enhanced efficiency in the removal of Cr(VI) ions from aqueous solutions compared with its natural form. The coefficient of determination (R^2 = 0.9902) for modified diatomite indicates a strong correlation between the Freundlich isotherm model and the experimental data (Figure 15). These findings underscore that while natural diatomite demonstrates moderate sorption efficiency, surface modifications substantially improve its adsorptive performance, making it a more effective sorbent for water treatment and heavy metal removal applications.

To further understand the sorption mechanisms, the Dubinin–Radushkevich isotherms were analyzed for the previously discussed sorbents. The data used to construct these isotherms are presented in Table 14.

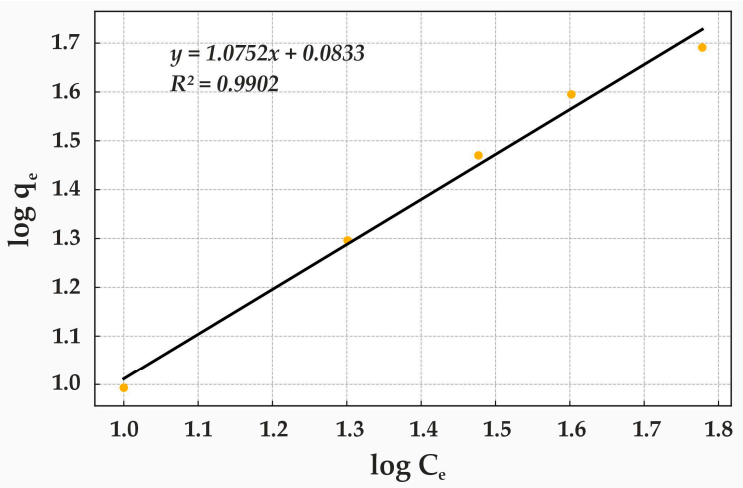


Figure 15. Freundlich adsorption isotherm for sorption onto modified diatomite.

Table 14. Data for the construction of the Dubinin–Radushkevich sorption isotherm for Lewatit MonoPlus M500.

q_e, mg/g	ε^2	ln q_e	ε	C_e, mol/L	C_e, mg/L
9.81	422	2.28	20.54	0.000250019	13
19.72	354	2.98	18.82	0.000500038	26
29.35	301	3.38	17.36	0.000903916	47
39.02	264	3.66	16.24	0.001423186	74
48.60	233	3.88	15.26	0.002115547	110
B_D, mol^2/kJ^2		ln q_D	q_{DR}, mg/g	E, kJ/mol	
0.0084		5.8756	356.238	7.751	

where q_e (mg/g) represents the equilibrium adsorption capacity; ε^2 is the squared Polanyi potential; ln q_e is the natural logarithm of q_e; ε is the Polanyi potential; C_e (mol/L) denotes the equilibrium concentration of the adsorbate in molar units; C_e (g/L) represents the equilibrium concentration of the adsorbate in grams per liter; B_D (mol^2/kJ^2) represents the Dubinin–Radushkevich isotherm constant; ln q_D is the natural logarithm of the Dubinin–Radushkevich adsorption capacity; q_{DR} (mg/g) is the Dubinin–Radushkevich adsorption capacity, and E (kJ/mol) denotes the mean free energy of adsorption.

The Dubinin–Radushkevich isotherm is commonly used to describe sorption processes occurring in the micropores of sorbents. For Lewatit MonoPlus M500, the equation takes the following form:

$$y = -0.0084x + 5.8756;\ R^2 = 0.9928 \quad (7)$$

where (y) represents the adsorption energy and corresponds to the logarithm of the equilibrium concentration or the volume of filled micropores, depending on the equation modification. The regression coefficients and the high determination coefficient indicate a strong correlation between the experimental data and the model, confirming the high predictive capability of this isotherm for the given sorption process (Figure 16).

The Dubinin–Radushkevich isotherm is widely applied to describe sorption mechanisms in microporous materials. The slope coefficient (−0.0084) represents the energy interaction between sorbate molecules and the sorbent, where its negative value indicates a decrease in adsorption energy with increasing pressure or adsorbate concentration. This behavior is characteristic of physisorption. The constant term (5.8756) corresponds to the maximum adsorption capacity of the sorbent and the energy required for micropore filling, where higher values indicate greater sorbent capacity.

The Dubinin–Radushkevich isotherm analysis confirms that sorption onto this sorbent exhibits high adsorption capacity at relatively low sorption energy, reinforcing the domi-

nance of physical adsorption. The strong determination coefficient (R^2) demonstrates a high correlation between the model and experimental data, validating the efficiency of Lewatit MonoPlus M500 in Cr(VI) removal (Figure 15). The polymeric composition and uniform particle distribution of this anion exchanger contribute to high stability and reproducibility of the sorption process.

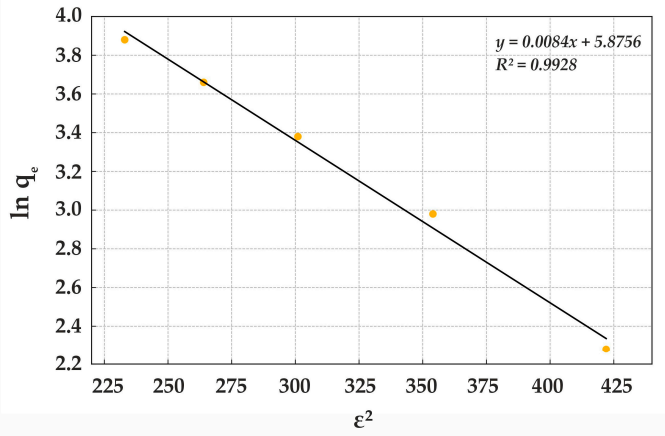


Figure 16. Dubinin–Radushkevich isotherm for Lewatit MonoPlus M500 sorption.

Thus, the Lewatit MonoPlus M500 anion exchanger is an effective sorbent, and the Dubinin–Radushkevich isotherm appropriately describes its sorption behavior. For natural diatomite, the applicability of the Dubinin–Radushkevich isotherm model further supports its microporous sorption characteristics. Table 15 presents the corresponding isotherm data.

Table 15. Data for the construction of the Dubinin–Radushkevich sorption isotherm for sorption onto natural diatomite.

q_e, mg/g	ε^2	ln q_e	ε	C_e, mol/L	C_e, g/L
4.92	133	1.59	11.51	0.00965	0.502
9.87	96	2.29	9.81	0.01944	1.011
14.7	78	2.69	8.83	0.02908	1.512
19.54	66	2.97	8.14	0.03889	2.022
24.35	58	3.19	7.60	0.04875	2.535
B_D, mol^2/kJ^2		ln q_D	q_{DR}, mg/g	E, kJ/mol	
0.212		4.374	79.36	4.86	

where q_e (mg/g) represents the equilibrium adsorption capacity; ε^2 is the squared Polanyi potential; ln q_e is the natural logarithm of q_e; ε is the Polanyi potential; C_e (mol/L) denotes the equilibrium concentration of the adsorbate in molar units; C_e (g/L) represents the equilibrium concentration of the adsorbate in grams per liter; B_D (mol^2/kJ^2) represents the Dubinin–Radushkevich isotherm constant; ln q_D is the natural logarithm of the Dubinin–Radushkevich adsorption capacity; q_{DR} (mg/g) is the Dubinin–Radushkevich adsorption capacity, and E (kJ/mol) denotes the mean free energy of adsorption.

A high determination coefficient indicates that the experimental data strongly correlates with the Dubinin–Radushkevich model. The low adsorption energy kJ/mol confirms that the process follows a physical adsorption mechanism. Natural diatomite effectively adsorbs contaminants due to its microporous structure, with adsorption occurring at a relatively low interaction energy. This makes it an efficient natural sorbent for pollutant removal at low and medium concentrations. However, to enhance adsorption efficiency, material modification may be necessary (Figure 17).

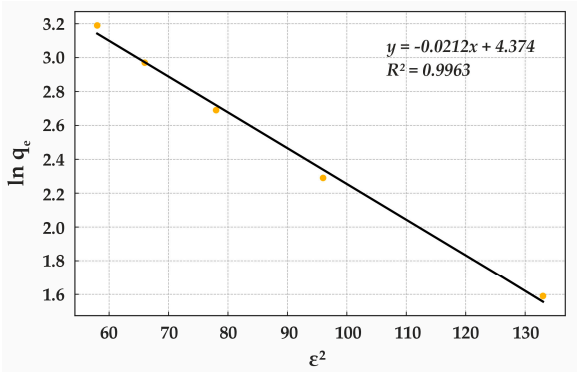


Figure 17. Dubinin–Radushkevich isotherm for natural diatomite.

Table 16 shows the data for the construction of the Dubinin–Radushkevich isotherm of sorption by modified diatomite.

Table 16. Data for the construction of the Dubinin–Radushkevich isotherm for sorption onto modified diatomite.

q_e, mg/g	ε^2	ln q_e	ε	C_e, mol/L	C_e, mg/L
9.84	449	2.29	21.19	0.000192322	10
19.78	379	2.98	19.47	0.000384645	20
29.52	341	3.39	18.47	0.000576967	30
39.36	315	3..67	17.76	0.00076929	40
49.10	281	389	16.75	0.001153935	60
B_D, mol^2/kJ^2		ln q_D	q_{DR}, mg/g		E, kJ/mol
0.0098		6.7046	819.998		0.495

where q_e (mg/g) represents the equilibrium adsorption capacity; ε^2 is the squared Polanyi potential; ln q_e is the natural logarithm of q_e; ε is the Polanyi potential; C_e (mol/L) denotes the equilibrium concentration of the adsorbate in molar units; and C_e (g/L) represents the equilibrium concentration of the adsorbate in grams per liter.

For modified diatomite, the determination coefficient indicates even better model accuracy compared with natural diatomite, suggesting that the modified material is better suited for micropore sorption. A decrease in the slope coefficient to −0.0098 reflects slightly lower adsorption energy, demonstrating that diatomite modification enhances its efficiency in physical adsorption due to improved pore structure (Figure 18).

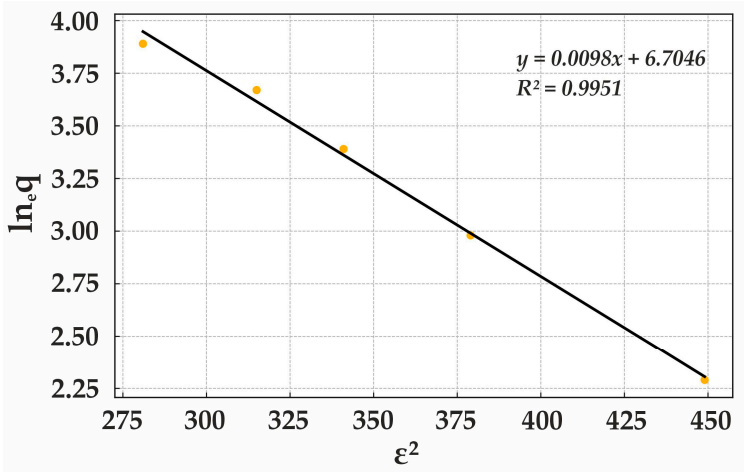


Figure 18. Dubinin–Radushkevich isotherm for modified diatomite.

This study evaluated the adsorption efficiency of various sorbents, including natural and Fe-modified diatomite, Lewatit ion-exchange resin, activated carbon, and taurite, for the removal of hexavalent chromium (Cr(VI)) from aqueous solutions. To provide a comprehensive assessment, a comparative analysis was conducted with previously published studies, systematically examining adsorption capacity, equilibrium time, and regeneration potential.

3.1. Activated Carbon: Adsorption Efficiency and Kinetics

The results indicate that activated carbon exhibited a Cr(VI) adsorption capacity of 112.7 mg/g under optimal conditions, which aligns with previous studies. Prior research has reported adsorption capacities ranging from 60 to 75 mg/g for activated carbon derived from sugarcane bagasse, with maximum efficiency achieved under acidic conditions [53]. Similarly, studies have documented an adsorption capacity of 93 mg/g for activated carbon produced from walnut shells under optimized conditions [54]. These findings confirm that activated carbon remains a widely utilized sorbent for Cr(VI) removal, with its efficiency being highly dependent on the precursor material and activation method.

A key advantage observed in the present study is the faster equilibrium time (90 min) compared with conventional activated carbon, which typically requires prolonged contact times due to pore diffusion limitations. This finding is consistent with [52], which reported that equilibrium for walnut shell-derived activated carbon was reached within 120 min. The enhanced adsorption kinetics observed in this study could be attributed to a higher density of active functional groups, promoting more rapid Cr(VI) uptake.

3.2. Lewatit MonoPlus M500: Adsorption Capacity and Stability

The adsorption capacity of Lewatit MonoPlus M500 was determined to be 288 mg/g, closely aligning with the values reported by [51], which documented adsorption capacities exceeding 150 mg/g for Lewatit resins. In both cases, the adsorption behavior followed the Langmuir isotherm, indicating monolayer adsorption on a homogeneous surface. In this study, Fe-modified diatomite demonstrated a significantly enhanced adsorption capacity of 256.41 mg/g, surpassing the 218.2 mg/g reported by [55] for Fe-doped composites. Studies such as [56,57] confirm that Cr(VI) adsorption is most effective in acidic environments, which is consistent with the findings of this study, where pH 4 was identified as the optimal condition for Fe-modified diatomite. The increase in adsorption capacity can be attributed to enhanced surface functionalization and a higher density of active adsorption sites, resulting from the optimized Fe(III) hydroxide precipitation process.

Furthermore, this study demonstrated that Fe-modified diatomite achieved adsorption equilibrium within 60 min, whereas previous studies have reported equilibrium times exceeding 120 min. The work of [58] on ion-exchange kinetics in inorganic sorbents highlighted that adsorption efficiency is highly influenced by surface modification and porosity. The observed enhancement in the adsorption efficiency of Fe-modified diatomite can be attributed to the greater availability of active binding sites, which aligns with the findings from previous research on surface modification and porosity effects. Additionally, while Kudryavtsev and Zilberman observed a strong correlation between the Dubinin–Radushkevich isotherm and microporous inorganic sorbents, the present study found that natural diatomite exhibited adsorption behavior best described by the Freundlich model, whereas Fe-modified diatomite followed the Langmuir isotherm, confirming its monolayer adsorption mechanism.

3.3. Comparison with Ion-Exchange Resins and Polymeric Sorbents

Studies by [59] investigated Cr(VI) adsorption using ion-exchange resins in continuous column experiments, demonstrating high efficiency in acidic environments, with

a maximum adsorption capacity of approximately 200 mg/g. Similarly, [51] reported high Cr(VI) removal efficiency using Lewatit anion-exchange resins, with a Langmuir adsorption capacity exceeding 150 mg/g. In comparison, Fe-modified diatomite exhibited a higher adsorption capacity of 256.41 mg/g, surpassing the performance of conventional ion-exchange resins under similar experimental conditions. Unlike synthetic resins, Fe-modified diatomite offers an eco-friendly and cost-effective alternative with promising regeneration potential.

The investigation [60] examined the adsorption efficiency of porous strong-base anion exchangers functionalized with N,N-dimethyl 2-hydroxyethyl ammonium and N,N-diethyl 2-hydroxyethyl ammonium groups for Cr(VI) removal. Their results showed high retention capacities (278.2–323.7 mg/g) with optimal sorption kinetics following the pseudo-second-order (PSO) model, supporting a chemisorption mechanism.

3.4. Industrial Implications and Practical Applications

Unlike commercial resins and activated carbons, which often experience irreversible fouling, Fe-modified diatomite exhibited excellent regeneration capacity. Experimental results demonstrated that after three adsorption–desorption cycles, Fe-modified diatomite retained over 90% of its initial adsorption capacity, reinforcing its potential for sustainable application in industrial wastewater treatment. This characteristic provides a significant advantage over Lewatit resins, which typically degrade after multiple reuse cycles due to polymer backbone deterioration [61].

4. Conclusions

Among the tested sorbents, modified diatomite and Lewatit MonoPlus M500 exhibited the highest sorption activity toward hexavalent chromium ions. It has been established that Fe modification induces significant alterations in surface morphology, forming irregular Fe-rich deposits that enhance adsorption. The chemical modification of diatomite with iron oxyhydroxides significantly enhanced its sorption properties by increasing sorption capacity and reducing adsorption energy, as confirmed by the high coefficient values in the Freundlich and Dubinin–Radushkevich isotherm models.

A key distinction of this study is the demonstration that Fe-modified diatomite can regenerate after desorption, restoring its original composition and structural integrity. This underscores its potential for reuse, which is a critical factor for industrial applications. Additionally, the ability to regenerate the diatomite's surface structure after its use in sorption processes allows for its repeated application as a matrix for iron compounds that actively interact with hexavalent chromium ions in solution. Lewatit MonoPlus M500 demonstrated efficient adsorption of chromate ions due to the presence of both strong and weak sorption centers, ensuring their applicability across a wide concentration range. Experimental data confirmed that the Freundlich and Dubinin–Radushkevich isotherms best describe adsorption processes in heterogeneous and microporous materials such as natural and modified diatomite.

Author Contributions: Conceptualization, D.F. and S.T.; methodology, D.F. and S.T.; software, K.S.; validation, Z.B. and N.B.; formal analysis, A.U.; investigation, Z.B. and N.B.; resources, B.K.; data curation, A.U.; writing—original draft preparation, D.F. and S.T.; writing—review and editing, D.F. and S.T.; visualization, K.S.; supervision, B.K.; project administration, A.U.; funding acquisition, B.K. All authors have read and agreed to the published version of the manuscript.

Funding: This study is supported by the Science Committee of the Ministry of Science and Higher Education of the Republic of Kazakhstan through Program -Targeted Funding BR21882140.

Data Availability Statement: Data are contained within the article.

Acknowledgments: We extend our gratitude to the Ministry of Science and Higher Education of the Republic of Kazakhstan.

Conflicts of Interest: The authors confirm the absence of any conflicts of interest.

References

1. Akhtar, N.; Syakir, I.M.I.; Bhawani, S.A.; Umar, K. Various Natural and Anthropogenic Factors Responsible for Water Quality Degradation: A Review. *Water* **2021**, *13*, 2660. [CrossRef]
2. Ukhurebor, K.E.; Aigbe, U.O.; Onyancha, R.B.; Nwankwo, W.; Osibote, O.A.; Paumo, H.K.; Ama, O.M.; Adetunji, C.O.; Siloko, I.U. Effect of hexavalent chromium on the environment and removal techniques: A review. *J. Environ. Manag.* **2021**, *280*, 111809. [CrossRef]
3. Owlad, M.; Aroua, M.K.; Daud, W.M.A.W.; Baroutian, S. Removal of hexavalent chromium-contaminated water and wastewater: A review. *Water Air Soil Pollut.* **2009**, *200*, 59–77. [CrossRef]
4. Irshad, M.A.; Sattar, S.; Nawaz, R.; Al-Hussain, S.A.; Rizwan, M.; Bukhari, A.; Waseem, M.; Irfan, A.; Inam, A.; Zaki, M.E.A. Enhancing chromium removal and recovery from industrial wastewater using sustainable and efficient nanomaterial: A review. *Ecotoxicol. Environ. Saf.* **2023**, *263*, 115231. [CrossRef]
5. Sarker, S.S.; Akter, T.; Parveen, S.; Uddin, M.T.; Mondal, A.K.; Sujan, S.M.A. Microalgae-based green approach for effective chromium removal from tannery effluent: A review. *Arab. J. Chem.* **2023**, *16*, 105085. [CrossRef]
6. Verma, B.; Balomajumder, C. Hexavalent chromium reduction from real electroplating wastewater by chemical precipitation. *Bull. Chem. Soc. Ethiop.* **2020**, *34*, 67–74. [CrossRef]
7. Sawicka, E.; Jurkowska, K.; Piwowar, A. Chromium (III) and chromium (VI) as important players in the induction of genotoxicity—Current view. *Ann. Agric. Environ. Med.* **2021**, *28*, 1–10. [CrossRef] [PubMed]
8. Krawic, C.; Zhitkovich, A. Chapter Two—Chemical mechanisms of DNA damage by carcinogenic chromium (VI). In *Advances in Pharmacology*; Academic Press: Cambridge, MA, USA, 2023; Volume 96, pp. 25–46. [CrossRef]
9. Keenan, C.E.; Kelleher, R.; Gray, S.G. Chapter 9—Environmental pollution, epigenetics, and cancer. In *Epigenetic Cancer Therapy. Translational Epigenetics*, 2nd ed.; Academic Press: London, UK, 2023; pp. 175–194. ISBN 978-0-323-91367-6. [CrossRef]
10. Wise, J.P.; Young, J.L.; Cai, J.; Cai, L. Current Understanding of Hexavalent Chromium [Cr (VI)] Neurotoxicity and New Perspectives. *Environ. Int.* **2022**, *158*, 106877. [CrossRef]
11. World Health Organisation. Chromium in Drinking-Water. Background Document for Development of WHO Guidelines for Drinking-Water Quality. Available online: https://cdn.who.int/media/docs/default-source/wash-documents/wash-chemicals/chromium.pdf?sfvrsn=37abd598_6 (accessed on 3 April 2024).
12. World Health Organisation. The World Health Report 2006: Working Together for Health. Available online: https://www.who.int/publications/i/item/9241563176 (accessed on 31 October 2006).
13. Faust, S.D.; Aly, O.M. *Chemistry of Water Treatment*; CRC Press Taylor & Francis Group: Boca Raton, FL, USA, 2018; ISBN 9781315139265. [CrossRef]
14. Sedlak, D.L.; Chan, P.G. Reduction of hexavalent chromium by ferrous iron. *Geochim. Cosmochim. Acta* **1997**, *61*, 2185–2192. [CrossRef]
15. Kenzhaliyev, B.; Ultarakova, A.; Toishybek, A.; Sadykov, N. Processing of Ilmenite Concentrate with High Chromium Content. *Processes* **2024**, *12*, 1462. [CrossRef]
16. Diatomite: Versatile and Unique. Available online: https://avestnik.kz/diatomit-universalnyiy-i-unikalnyiy/ (accessed on 17 October 2024).
17. Mohamedbakr, H.G. Diatomite: Its characterisation, modifications and applications. *Asian J. Mater. Sci.* **2010**, *2*, 121–136. [CrossRef]
18. Morrow, B.A.; McFarlan, A.J. Chemical reactions at silica surfaces. *J. Non-Cryst. Solids* **1990**, *120*, 61–71. [CrossRef]
19. Marketpublishers. Review of the American Diatomite Market. Available online: https://marketpublishers.ru/lists/12087/news.html (accessed on 11 October 2024).
20. Surkova, T.; Abdikerim, B.; Berkinbayeva, A.; Azlan, M.; Baltabekova, Z. Obtaining modified sorbents based on natural raw materials of Kazakhstan and research of their properties. *Kompleks. Ispolz. Miner. Syra = Complex Use Miner. Resour.* **2022**, *322*, 23–32. [CrossRef]
21. Myrzalieva, S.; Bagasharova, Z.; Akilbekova, S. Study of the possibility of using zeolite and diatomite in the treatment of oil-contaminated wastewater. *Kompleks. Ispolz. Miner. Syra = Complex Use Miner. Resour.* **2022**, *322*, 33–42. [CrossRef]
22. Kuldeev, E.; Bondarenko, I.; Temirova, S.; Tastanov, E.; Nurlybaev, R. Composition and properties of diatomite raw materials of Kazakhstan and synthesis of silicalcites on its basis for obtaining construction products. *Kompleks. Ispolz. Miner. Syra = Complex Use Miner. Resour.* **2018**, *4*, 149–157. [CrossRef]

23. Kuldeyev, E.; Bondarenko, I.; Abdulvaliyev, R.; Temirova, S.; Abdikerim, B. Processing of low quality ekibastuz coals ashes and natural diatomites to obtain alumina and foamed glass. *Metalurgija* **2020**, *3*, 351–354.
24. Kenzhaliev, B.; Kuldeev, E.; Luganov, V.; Bondarenko, I.; Motovilov, I.; Temirova, S. Production of Very Fine Spherical Particles of Ferriferous Pigments from the Diatomaceous Raw Material of Kazakhstan. *Glass Ceram.* **2019**, *76*, 194–198. [CrossRef]
25. Kuldeyev, E.; Tastanova, A.; Bondarenko, I.; Temirova, S.; Nurlybayev, R.; Botantayeva, B.; Zaihidee, F. Complex alumina-ferrous coagulant for effective wastewater purification from hydro-gen sulfide. *Adv. Mater. Sci. Eng.* **2021**, *1*, 5595599. [CrossRef]
26. Memedi, H.; Atkovska, K.; Kuvendziev, S.; Garai, M.; Marinkovski, M.; Dimitrovski, D.; Pavlovski, B.; Reka, A.A.; Lisichkov, K. Chapter 9—Removal of Chromium(VI) from Aqueous Solution by Clayey Diatomite: Kinetic and Equilibrium Study. In *Contaminant Levels and Ecological Effects*; Balabanova, B., Stafilov, T., Eds.; Springer: Cham, Switzerland, 2021; pp. 263–282. ISBN 978-3-030-66134-2. [CrossRef]
27. Sungworawongpana, S.; Pengprecha, S. Calcination Effect of Diatomite to Chromate Adsorption. *Procedia Eng.* **2011**, *8*, 53–57. [CrossRef]
28. Ghobara, M.M.; Ghobara, M.M.; Ghobara, M.M.; Mohamed, A. Diatomite in use: Nature, modifications, commercial applications and prospective trends. In *Diatoms: Biology and Applications*, 1st ed.; Wiley-Scrivener Publisher: Beverly, MA, USA, 2019; pp. 471–509. ISBN 9781119370741. [CrossRef]
29. Fathy, N.A.; Mousa, S.M.; Aboelenin, R.M.; Sherief, M.A.; Abdelmoaty, A.S. Strengthening the surface and adsorption properties of diatomite for the removal of Cr (VI) and methylene blue dye. *Arab. J. Geosci.* **2022**, *15*, 1664–1675. [CrossRef]
30. Lemessa, G.; Chebude, Y.; Alemeyahu, E. Adsorptive removal of Cr (VI) from wastewater using magnetite-diatomite nanocomposite. *AQUA Water Infrastruct. Ecosyst. Soc.* **2023**, *72*, 2239–2261. [CrossRef]
31. Lu, J.W.; Fu, F.L.; Zhang, L.; Tang, B. Insight into efficient co-removal of Se (IV) and Cr (VI) by magnetic mesoporous carbon microspheres: Performance and mechanism. *Chem. Eng. J.* **2018**, *346*, 590–599. [CrossRef]
32. Yuan, P.; Liu, D.; Fan, M.; Yang, D.; Zhu, R.; Ge, F.; Zhu, J.; He, H. Removal of hexavalent chromium [Cr (VI)] from aqueous solutions by the diatomite-supported/unsupported magnetite nanoparticles. *J. Hazard. Mater.* **2010**, *173*, 614–621. [CrossRef]
33. Danh, H.T.; Ly Nguyen-Thi, T.; Nguyen, V.; Khieu, D.Q.; Du, P.D. Removal of Pb (II) from Aqueous Solutions with Manganese Oxide-Modified Diatomite. *Adsorpt. Sci. Technol.* **2023**, *2023*, 7744896. [CrossRef]
34. Jiang, L.; Liu, L.; Xiao, S.; Chen, J. Preparation of a novel manganese oxide-modified diatomite and its aniline removal mechanism from solution. *Chem. Eng. J.* **2016**, *284*, 609–619. [CrossRef]
35. Al-Ghouti, M.A.; Al-Degs, Y.S.; Khraisheh, M.A.M.; Ahmad, M.N.; Allen, S.J. Mechanisms and chemistry of dye adsorption on manganese oxides-modified diatomite. *J. Environ. Manag.* **2009**, *90*, 3520–3527. [CrossRef]
36. Islam, M.A.; Angove, M.J.; Morton, D.W. Recent innovative research on chromium (VI) adsorption mechanism. *Environ. Nanotechnol. Monit. Manag.* **2019**, *12*, 100267. [CrossRef]
37. Fenti, A.; Chianese, S.; Iovino, P.; Musmarra, D.; Salvestrini, S. Cr(VI) Sorption from Aqueous Solution: A Review. *Appl. Sci.* **2020**, *10*, 6477. [CrossRef]
38. Mutabazi, E.; Qiu, X.; Song, Y.; Li, C.; Jia, X.; Hakizimana, I.; Niu, J.; Nuramkhaan, M.; Zhao, Y. Cr (VI) adsorption on activated carbon, sludge derived biochar, and peanut shells derived biochar: Performance, mechanisms during the reuse process and site energy distribution analysis. *J. Water Process Eng.* **2024**, *57*, 104679. [CrossRef]
39. Mallik, A.K.; Moktadir, M.A.; Rahman, M.A.; Shahruzzaman, M.; Rahman, M.M. Progress in surface-modified silicas for Cr (VI) adsorption: A review. *J. Hazard. Mater.* **2022**, *423*, 127041. [CrossRef]
40. Gorno-Rudnaya Kompaniya Koksu, TOO. Available online: https://kz.all.biz/taurit-tauritovye-koncentraty-g273236 (accessed on 17 October 2024).
41. Moshnikov, I.A.; Kovalevskii, V.V. Electrophysical properties of shungites at low temperatures. *Nanosyst. Phys. Chem. Math.* **2016**, *7*, 214–219. [CrossRef]
42. Kovalevski, V.V.; Kochneva, I.V.; Rozhkova, V.S. Sorption Properties of Natural and Modified Shungite Rocks Differing in Origin. *Inorg. Mater.* **2023**, *59*, 736–741. [CrossRef]
43. Ongarbayev, Y.; Baigulbayeva, M.; Tileuberdi, Y.; Zhumakhan, K. Sorption of Oil by Mechanochemicaly Activated Shungite. *Rud.-Geološko-Naft. Zb.* **2022**, *37*, 4. [CrossRef]
44. Semenkova, A.; Belousov, P.; Rzhevskaia, A.; Izosimova, Y.; Maslakov, K.; Tolpeshta, I.; Romanchuk, A.; Krupskaya, V. U(VI) sorption onto natural sorbents. *J. Radioanal. Nucl. Chem.* **2020**, *326*, 293–301. [CrossRef]
45. Skorobogatov, G.A.; Ashmarova, Y.A.; Rebrova, A.G. Transformations of shungite in aqueous media (pH from 1 to 12). *Russ. J. Appl. Chem.* **2017**, *90*, 113–119. [CrossRef]
46. Han, S.; Zang, Y.; Gao, Y.; Yue, Q.; Zhang, P.; Kong, W.; Jin, B.; Xu, X.; Gao, B. Co-monomer polymer anion exchange resin for removing Cr (VI) contaminants: Adsorption kinetics, mechanism and performance. *Sci. Total Environ.* **2020**, *709*, 136002. [CrossRef] [PubMed]
47. Verma, R.; Maji, P.K.; Sarkar, S. Detailed investigation of effective trace Cr (VI) removal mechanism by anion exchange resin with phenol-formaldehyde matrix. *J. Ind. Eng. Chem.* **2022**, *111*, 147–154. [CrossRef]

48. Kahraman, H.T.; Pehlivan, E. Evaluation of anion-exchange resins on the removal of Cr (VI) polluted water: Batch ion-exchange modelling. *Arab. J. Geosci.* **2019**, *12*, 532. [CrossRef]
49. Ali, A.; Sadia, M.; Azeem, M.; Ahmad, M.Z.; Umar, M.; Ul Abbas, Z. Ion Exchange Resins and their Applications in Water Treatment and Pollutants Removal from Environment: A Review: Ion Exchange Resins and their Applications. *Futur. Biotechnol.* **2023**, *3*, 12–19. [CrossRef]
50. Yamanaka, K. Ion-Exchange Resins. In *Encyclopedia of Polymeric Nanomaterials*; Kobayashi, S., Müllen, K., Eds.; Springer: Berlin/Heidelberg, Germany, 2015; ISBN 978-3-642-29648-2. [CrossRef]
51. Pehlivan, E.; Cetin, S. Sorption of Cr (VI) ions on two Lewatit-anion exchange resins and their quantitative determination using UV-visible spectrophotometer. *J. Hazard. Mater.* **2009**, *163*, 448–453. [CrossRef]
52. Gode, F.; Pehlivan, E. Removal of Cr (VI) from aqueous solution by two Lewatit-anion exchange resins. *J. Hazard. Mater.* **2005**, *119*, 175–182. [CrossRef] [PubMed]
53. Luo, X.; Cai, Y.; Liu, L.; Zeng, J. Cr (VI) adsorption performance and mechanism of an effective activated carbon pre-pared from bagasse with a one-step pyrolysis and $ZnCl_2$ activation method. *Cellulose* **2019**, *26*, 4921–4934. [CrossRef]
54. Yazid, H.; Bouzid, T.; El mouchtari, E.M.; Bahsis, L.; El Himri, M.; Rafqah, S.; El haddad, M. Insights into the Adsorption of Cr(VI) on Activated Carbon Prepared from Walnut Shells: Combining Response Surface Methodology with Com-putational Calculation. *Clean Technol.* **2024**, *6*, 199–220. [CrossRef]
55. Zhang, Z.; Song, Z.; Luo, C.; Zhao, H.; Yang, L.; Jia, H.; Huang, H.; Zhao, X. Synthesis, Char-acterization and Application of Ferrous Iron-Embedded Schwertmannite for Cr (VI) Reduction–Adsorption from Aqueous Solutions. *Int. J. Environ. Res.* **2024**, *18*, 16. [CrossRef]
56. Hezil, N.; Fellah, M.; Assala, O.; Touhami, M.Z.; Guerfi, K. Elimination of Chromium (VI) by Adsorption onto Natural and/or Modified Kaolinite. *Diffus. Found.* **2018**, *18*, 106–112. [CrossRef]
57. Oliveira, J.C.G.; de Moraes Ferreira, R.; Stapelfeldt, D.M.A. Use of *Salvinia* sp. on the Adsorption of Hexavalent Chromium. *Environ. Sci. Pollut. Res.* **2019**, *26*, 30463–30471. [CrossRef]
58. Kudryavtsev, P.; Zilberman, M. Kinetics of ion exchange on inorganic sorbents. *Int. J. Hydrol.* **2023**, *7*, 91–117. [CrossRef]
59. Ponnaiah, G.P.; Konga, A.K. Continuous Column Study of Chromium (VI) Adsorption by Ion Exchange Resin. *ETCE* **2014**, *1*, 2.
60. Dragan, E.S.; Humelnicu, D.; Dinu, M.V. Design of porous strong base anion exchangers bearing N,N-dialkyl 2-hydroxyethyl ammonium groups with enhanced retention of Cr(VI) ions from aqueous solution. *React. Funct. Polym.* **2018**, *124*, 55–63. [CrossRef]
61. Cobzaru, C.; Inglezakis, V. Chapter Ten—Ion Exchange. In *Progress in Filtration and Separation*; Academic Press: Cambridge, MA, USA, 2015; pp. 425–498. [CrossRef]

Disclaimer/Publisher's Note: The statements, opinions and data contained in all publications are solely those of the individual author(s) and contributor(s) and not of MDPI and/or the editor(s). MDPI and/or the editor(s) disclaim responsibility for any injury to people or property resulting from any ideas, methods, instructions or products referred to in the content.